

Long-term variations in nearshore wave climate and littoral drift at Ganpatipule coast, eastern Arabian Sea and its link to Pacific climate variability

Jesbin George^{1,2}, V. Sanil Kumar^{1*}

¹Ocean Engineering, CSIR-National Institute of Oceanography (Council of Scientific & Industrial Research), Dona Paula, Goa 403 004 India

²Research Scholar, Department of Marine Science, Bharathidasan University, Tiruchirappalli 620023 Tamil Nadu, India

*corresponding author Tel: 0091 832 2450 327 email:sanil@nio.org

Abstract

Nearshore wave characteristics and its variations at Ganpatipule coast, eastern Arabian Sea for the past four decades (1979-2016) have been examined. The study is based on ERA-Interim wave data at ~50 m water depth and the nearshore wave parameters estimated using the numerical model SWAN (Simulating WAVes Nearshore), executed from the Delft3D dashboard considering shallow water wave propagation, wave set-up, and breaking. The littoral drift is estimated based on bulk transport formula of Coastal Engineering Research Centre with the input from the hydrodynamic module. The model shows good agreement with wave rider buoy measured wave parameters at 14-m water depth. Anomalies of breaker height, period and direction vary in the range of -0.35 to 0.4 m, -0.80 to 1 s and -16 to 12° respectively during the study period. A detailed analysis of monthly variations of breaker height along the study region suggests a significant increasing trend during the Asian summer monsoon (JJAS), whereas a decreasing trend is identified during the non-monsoon period. The study region accounts for a northerly net transport of $3.9 \times 10^5 \text{ m}^3 \text{ yr}^{-1}$ with a significant increasing trend of $1840 \text{ m}^3 \text{ yr}^{-1}$. The strong wind field region along the central Arabian Sea (65-70°E and 15-20°N) gives a strengthened positive correlation ($r > 0.7$) with the littoral drift. Impact of Pacific climate variability on interannual and decadal timescales are observed in the littoral drift rates.

Keywords: Wave characteristics, littoral drift, coastal processes, long-term changes, Pacific climate variability.

Key points

- Investigates nearshore wave climate and littoral drift for past four decades (1979-2016) at a location in eastern Arabian Sea
- Breaker height shows a significant increasing trend during the Asian Summer monsoon (JJAS)
- An increasing trend in the net littoral drift is observed ($1840 \text{ m}^3 \text{ yr}^{-1}$)

Impact of Pacific climate variability on littoral drift is observed during 1979-1989y.

1. Introduction

Knowledge of broad-scale coastal dynamics is required to plan coastal engineering works. Nearshore waves are the principal component of coastal dynamics, and its variation is to be quantified due to the changes in the wind pattern due to climate change (Chini et al., 2010). Coastal processes are governed by the strong depth-induced dissipation processes of waves. The waves reaching the coastline at an oblique angle dissipate the energy in the surf zone and initiate littoral drift (also termed as longshore sediment transport, LST). Climate change-induced erosion is one of the most serious impacts being faced by the coastal system worldwide and is triggered by several physical drivers, particularly by variations in wave height and directions which leads to unbalanced sediment budget (Toimil et al., 2017). Seasonal-scale shoreline evolution has been previously reported by Thom and Hall (1991) and is linked to variations in wave height. Hemer et al. (2010) highlighted the importance of studying the impact of atmospheric systems on the nearshore wave climate. Even though researchers investigated climate change impacts on longshore sediment transport in the past (e.g., Adams et al., 2011; Casas-Prat et al., 2016; Casas-Prat and Sierra, 2012; Splinter et al., 2012), effects of changing climate on nearshore wave characteristics and the resulting regional littoral drift in the tropical regions are barely understood (Short, 2012). Thus there is a necessity to understand long-term variations in nearshore wave characteristics and littoral drift rates in the changing climate scenario. To examine long-term variations in nearshore characteristics, suitable long-term directional wave records are needed (Splinter et al., 2012). Generally, the acceptable time frame for analysing the parameters for climate change studies is ~ 30 years (IPCC, 2013).

North Indian Ocean wave climate is very dynamic due to the seasonally reversing monsoonal winds (Anoop et al., 2015). Previously long-term data exceeding 30-year time span has not been available to study the nearshore waves in the eastern Arabian Sea. With the availability of the global reanalysis dataset from European Centre for Medium-Range Weather Forecasts (ECMWF) Re-Analysis-Interim (ERA-I) (Dee et al., 2011), now it is possible to study the long-term changes in different atmospheric and ocean parameters. Several researchers (e.g., Harley et al., 2010; Hemer et al., 2010; Kumar et al., 2016) across the globe has used ERA-I datasets to examine the interannual wave climate variability. Previous studies along the eastern Arabian sea (Kumar and Naseef, 2015; Shanas and Sanil Kumar, 2014 b,c) suggests that ERA-I datasets give a good agreement with the measured data.

Investigating the long-term variations in wave climate and the causes which induce those variabilities are of keen interest to the scientists across the world (e.g., Dodet et al., 2010; Gallagher

et al., 2014; Weisse and Günther, 2007, Wandres et al., 2018). For a better understanding of the long-term wave climate of a region, it is essential to understand the atmospheric circulation patterns which drive the wave climate and its variability (Wandres et al., 2018). These circulation patterns and their variabilities can be very well described using climate indices. Several researchers studied interannual variability of wave climate and their response to well-known climate indices (e.g, Hemer et al., 2010; Izaguirre et al., 2011; Splinter et al., 2012). For coastal and ocean engineering applications, the relationship between wave climate variability and teleconnection patterns along the Atlantic, Pacific and the Indian Ocean were discussed by many (Izaguirre et al., 2011, 2010; Kumar et al., 2016; Semedo et al., 2011; Shimura et al., 2013). Earlier studies have shown that on interannual time scales, the Pacific Ocean variability modulates Indian Ocean (Du et al., 2009). The most prominent interannual mode of climate variability, El Niño–Southern Oscillation (ENSO), influences the Indian Ocean through the Walker circulation (Klein et al., 1999). The regional influence of ENSO is the increase in sea surface temperature and the reduction of wind speeds (Wyrki, 1981). Since winds are the generating force for the waves, the variabilities in wind anomalies caused by ENSO induce variations in wave climate (Schott et al., 2009). Another pattern of Pacific climate variability is Pacific Decadal Oscillation (PDO), described as a long-lived El- Niño like pattern on both interannual and decadal timescales (Newman et al., 2003). PDO, introduced by Mantua et al. (1997), is the leading orthogonal function of North Pacific (20°-70°N) SST monthly averaged anomalies, defined as departures from the climatological annual cycle after removing the global mean SST (Newman et al., 2016). The teleconnection between Pacific climate variability with Asian Summer Monsoon was investigated by several researchers (e.g., Krishnamurthy and Krishnamurthy, 2014; Krishnan and Sugi, 2003; Webster and Yang, 1992). A warm (cold) phase of PDO is associated with deficit (excess) rainfall (Krishnamurthy and Krishnamurthy, 2014) and a corresponding increase (decrease) in the surface air temperature over the Indian subcontinent (Krishnan and Sugi, 2003). Impact of ENSO and PDO on surface waves were investigated by Kumar et al. (2016). However, across the North Indian Ocean, there have been limited studies on the impacts of regional atmospheric circulation patterns (Indian Ocean Dipole) on the wave climate (Anoop et al., 2016).

The long-term changes in the nearshore waves and littoral drift in the eastern Arabian Sea, which forms the part of the central west coast of India, with time-series data at high temporal resolutions (6-h) is not attempted earlier. The aim of the study is to identify the; (1) interannual and seasonal variations in nearshore wave climate and littoral drift, (2) long-term trends in the nearshore wave climate and the littoral drift and the influence of Pacific climate variability in these trends. The article is organised as follows: Section 2 gives background information about the data and methods

used, Section 3 is about model validation and comparison. The results are discussed in section 4, followed by conclusions in section 5.

2. Data and Methods

The bathymetry of the study area (Figure 1) is obtained by merging the measured nearshore bathymetry data from 1 to 9 m water depth during December 2014 with the data from hydrographic chart No. 2028 (National Hydrographic Office, India 2004). Data of significant wave height (SWH), mean wave period and mean wave direction at the six-hour interval for 38 years (1979-2016) obtained from (ERA-I) with a spatial resolution of $0.5^\circ \times 0.5^\circ$ is used as an input to the numerical model. The data were extracted for the grid cell that encompasses the offshore boundary (~50 m water depth) of the model domain and, using a numerical model the waves were propagated from deep water to the breaker point with a temporal resolution of one hour. The numerical model SWAN (Simulating Waves Nearshore) (Booij et al., 1999), executed from the Delft3D (Hydraulics, 2006) dashboard considering shallow water wave propagation, wave set-up, and breaking is used for the nearshore wave transformation. The wave transformation model, grid generation and attributes and input parameters are similar to the one described in Shanias and Kumar (2014a) and Sanil Kumar et al. (2017). Apart from the wave parameters, other input variables used in the model were JONSWAP bottom friction coefficient which is taken as $0.067 \text{ m}^2/\text{s}^3$ (Hasselmann et al., 1973), Alpha (1) and Gamma (0.73) for depth induced breaking (Battjes and Stive, 1985) and non-linear triad interactions based on Lumped Triad Approximation model (LTA; Eldeberky, 1997) with Alpha and Beta are 0.1 and 2.2 respectively. Though, a revised value ($0.038 \text{ m}^2/\text{s}^3$) for bottom friction coefficient for wind-sea and swell conditions were recommended by Vledder et al. (2012), along the shallow waters of central west coast of India, wave transformation models with an input of $0.067 \text{ m}^2/\text{s}^3$ for bottom friction has performed well (e.g., Sanil Kumar et al., 2017; Shanias and Kumar, 2014a). Our simulations with these two different coefficients in January 2011 also shows a smaller variation (less than 7%) within the breaker heights. The model simulations were carried out in stationary mode, as recommended by Hydraulics (2006), for small domains of less than 100 km or 1 deg resolution which has an instantaneous wave propagation across the domain (Rogers et al., 2007). The directional resolution of the model is 10 degrees and has 24 frequencies between 0.05 – 1 Hz.

The study domain is first divided into a larger rectangular grid of 375×500 grid points with a grid spacing of 75 m each along x and y-direction. Another small rectangular grid was also created along the study region with 500×500 grid points at a grid spacing of 10 m and 15 m (along x and y-direction respectively). This smaller grid with higher resolution is nested into the larger grid with lower resolution. The model has three boundaries; 1) open boundary to the west from where the

waves propagate to the given domain, 2) closed boundary to the east (land) and 3) lateral boundaries at the north and south. The deepwater wave parameters were applied to all three boundaries. Since these wave conditions along the lateral sides of the grid is not necessarily a good approximation, the domain was created with sufficient distance on either side as suggested by Mortlock et al. (2014) to minimise the propagation of lateral boundary errors to the area of interest. Along the offshore boundary of the grid, there is a bit spatial variations in the wave parameters. However, along the central west of India, studies by Kumar et al. (2012) suggests that daily averaged wave parameters do not vary significantly within ~200 km distances. Also, Anoop et al. (2014) suggest that temporal variations are less than 10% for the wave parameters within a distance of 270 km and during higher sea state their characteristics were similar. Since our model domain and boundaries are small (~ 60 x 70 km) these variations can be negligible. The average spring tidal range in the study area is about 2 m and the average neap tidal range is 0.6 m. The sea level change by the tide and the change in water depth due to wave setup are not considered in the model simulation. The model simulations were carried out for 38 years (1979-2016) and the transformed breaking wave characteristics were extracted (star in Figure 1) by applying the breaking criteria ($H_b/h_b = 0.78$; CERC, 1984), where H_b is the breaker height and h_b is the breaking depth. The ratio between SWH and water depth was checked and when it is 0.78, the values were extracted at that grid point in the computational domain. This extracted wave component is used as input to the bulk formulae to estimate the littoral drift rate along the study region.

To estimate the littoral drift rate at Ganpatipule coast, a commonly used bulk formula suggested by U.S Army Corps of Engineers (CERC, 1984) is used. This formula relates wave energy flux with the immersed weight of the transported sediment and is expressed as,

$$I = KE C_{g,br} \sin \theta_{br} \cos \theta_{br} \quad (1)$$

Where I is the Immersed weight of LST rate, K is an empirical coefficient equal to 0.77 to be adopted with the root mean square wave height at breaker ($H_{rms,br}$). E is the wave energy at the breaker, $C_{g,br}$ is the group velocity at the breaker and θ is the angle between breaking wave crest and local shoreline (deg). With $SWH = 1.414 H_{rms,br}$, ρ_s = density of sediment (taken as 2650 kg/m³), porosity of sand (p) of 0.4, ρ_w = density of seawater (taken as 1030 kg/m³), $C_{g,br} \approx C = \sqrt{gh_{br}}$ and breaker index $K_i = (H_b/h_b)$, Eq. (1) is re-written as,

$$Q = 0.023 \sqrt{\frac{g}{K_i}} H_b^{2.5} \sin (2\theta) \quad (2)$$

Where Q is the LST in volume per unit time, g is the acceleration due to gravity (9.81 m/s^2), and H_b is the breaking wave height (m).

Along the central west coast of India, Sanil Kumar et al. (2017) and Shanas and Sanil Kumar (2014a) suggested bulk formulation based on Kamphuis (2002) which includes wave period, sediment grain size and beach slope to be reliable for estimating LST. In the present study to investigate long-term variations in littoral drift, long-term measured data of sediment size were not available and hence CERC formula is used. CERC formula is valid for sandy beaches (Van Rijn, 2014) and is widely accepted to compute long-term LST (Silva et al., 2012). However, it is important to realize that LST rates computed using the CERC approach are subject to a considerable degree of uncertainty (e.g., Kamphuis, 2000; Silva et al., 2012). Silva et al. (2012) estimated the uncertainties related to adoption of using different empirical constants in the CERC and other bulk LST formulas, and suggested that different approaches influence the magnitude of LST rates but gives a very limited impact on temporal LST variability pattern, which is one of the aims of the present study. The LST rates estimated using CERC approach is compared with the measured LST rates along the central west coast of India acquired by Kumar et al. (2003). They measured the lateral and vertical distribution of sediment transport rate with traps deployed in the line spanning the surf zone during February to May 1990 and reported an average gross transport rate of $726 \text{ m}^3 \text{ day}^{-1}$. In the present study, average gross transport estimated from February to May of 1990 using CERC with input parameters from the model simulations was $1650 \text{ m}^3 \text{ day}^{-1}$, which are more than double of the measured. Shanas and Sanil Kumar (2014a) compared the estimated LST rate using CERC with Kamphuis formulae, and a correction factor of 0.38 was recommended which gives a closer agreement with the target value of LST for the west coast of India. After incorporating this correction factor of 0.38 (i.e. values obtained from Eq. 2 are multiplied by 0.38) suggested by Shanas and Sanil Kumar (2014a), the estimated littoral drift is in closer agreement ($627 \text{ m}^3 \text{ day}^{-1}$) with the measured value ($726 \text{ m}^3 \text{ day}^{-1}$). The estimated sediment transport rates presented in this paper are based on this correction factor.

Wave characteristics from three points with a spatial distance of $\sim 4 \text{ km}$ at 4 m water depths along the Ganpatipule coast were extracted to study the spatial variation of the longshore component of wave power using the following equation.

$$P = \frac{1}{8} \rho_w g H_b^2 C \sin(\theta) \cos(\theta) \quad (3)$$

Where, P is the alongshore wave power (W/m), and C is the wave speed.

The earlier studies in the eastern Arabian Sea indicate that the wave characteristics can be described by grouping into 3 seasons; i) February-May (FMAM) is the pre-monsoon period in which wind-seas from the northwest are predominant, ii) June-September (JJAS) is the period of strong westerly waves due to the Indian summer/southwest monsoon (hereafter monsoon) and iii) October-January (ONDJ) is the post-monsoon period in which long-period swells from south and southwest are predominant (Amrutha et al., 2019; Glejin et al., 2013; Sanil Kumar and Anoop, 2015; Kumar et al., 2014). Since the waves in the study area vary during the different seasons, in the present study, waves during three seasons are examined. The measured wave characteristics at 14 m water depth during FMAM indicates that waves are with SWH less than 1.5 m and two predominant wave direction is observed (Figure 2, a, b). Waves with peak wave period less than 8 s are from 300 to 315° and long-period waves are from 225 to 240°. During JJAS, waves are with SWH ranging from 1 to 4 m and are from 240 to 270°. During ONDJ, waves are mainly from 225 to 240° and are mainly swells with peak wave period more than 8 s.

3. Comparison and validation of wave transformation model

Model simulations along the study region were performed by using ERA-I reanalysis wave data as offshore forcing. To compare and validate the performance of the model, measured wave data at 14 m water depth for a period of two years (2011-2012) is used. The skill of the model is determined based on the amount of deviation, which is measured by root-mean-square-error (RMSE) and bias, between the model results and observational data and correlation coefficient (R). After validation, the model shows a good comparison with the measured height and period data (Figure 3). Since the domain is small, the wind-wave growth over the region is minimal and hence the same is not considered in the present study. The model validation clearly indicates that the model reliably reproduces the wave condition of the region as it propagates from the deep water (50 m depth) to the buoy location (14 m) pointing out the insignificant wind-wave growth over the small study domain. Taking into account of all time instants of model simulations and buoy data during the years 2011 and 2012, the wave height under predicts by 16% and 10%, whereas, wave period over-predicts by 7% and 14% respectively. However, substantial differences in wave direction between the modelled and buoy were observed, especially during the non-monsoon period. This difference is due to the co-existence of wind-seas and swells along the study region where ERA-I data not likely to capture all the wind-seas (Kumar and Naseef, 2015), which could be important for the wave transformation model as even the lowest frequency wave could significantly contribute to these variations. This is clearly evident from Figure 2 c-e, where the swells (Figure 2, c) along the region during all the three seasons are likely captured by the ERA- I data (Figure 2,e), whereas the north-westerly waves

(Figure 2, d) during the pre and post-monsoon seasons are poorly represented in ERA- I data (Figure 2,e). During 2011, the measured and model results of SWH, period and direction shows a bias of -0.2 m, 0.44 s and -8° respectively and RMSE of 0.33 m, 0.8 s, and 28° respectively. During 2012, the bias values are -0.17 m, 0.63 s and -5° and RMSE values are 0.36 m, 1.07s and 28° respectively for SWH, period and direction. The R values between modelled and measured SWH, period and direction during the year 2011 and 2012 are 0.94, 0.81 and 0.5 and 0.88, 0.63 and 0.43 respectively. The bias values between modelled and measured wave parameters show variations during different seasons with its maximum variation in SWH during monsoon for both years and larger variations in wave period and wave direction during the post-monsoon season (Table 1).

4. Results and Discussions

4.1. Nearshore wave characteristics

The directional occurrence of breaking wave heights and mean wave periods for different months are shown in Figure 4. It is observed that during pre and post-monsoon, breaking wave height (H_b) generally varies in a narrow range (0.1 – 1.2 m), whereas during monsoon, H_b varies in large range (0.3 – 2.3 m). Monthly averaged H_b is maximum (1.67 m) during the month of July whereas it is minimum (0.40 m) during December. The averaged values of H_b is lowest (~ 0.47 m) during the post-monsoon and is maximum (1.33 m) during monsoon, whereas during post-monsoon average H_b is 0.67 m. Previous studies along the central west coast of India (e.g., Sanil Kumar et al., 2017; Shanas and Sanil Kumar, 2014a) also reported similar ranges in H_b during monsoon and non-monsoon period. Along the study domain from 1979 to 2016, only for $\sim 2\%$ of the time, wave height exceeds 2 m at the breaker zone with $\sim 88\%$ of occurrence along the direction $240-245^\circ$. About 47% time, wave breaks in the range of 0.5- 1 m with predominant ($\sim 39\%$) wave direction of $240-250^\circ$. Breaker heights ranging from 1- 2 m were observed $\sim 24\%$ times with its predominant ($\sim 65\%$ of the time) wave direction of $240-245^\circ$. Lower breaking heights (< 0.5 m) of the non-monsoon period were observed for about 25% times with the predominant ($\sim 49\%$) direction along $220-240^\circ$. Based on 1-year data, Sharma et al. (2017) reported that the predominant wave direction along Ganpatipule coast during monsoon ($\sim 35\%$) and non-monsoon ($\sim 53\%$) is $225-240^\circ$, whereas the present study shows a slight ($\sim 5^\circ$) increase in the direction.

Since the coastline along the study region is inclined 15° to the west with respect to the true north, the wave direction less than 255° is considered to be approaching from the south, whereas direction larger than 255° is considered to be approaching from the north. The breaker angle (α_b), which is the difference between mean wave direction and the direction normal to the depth contour

(255°), mostly persisted in between -15 and 25° during the study period. Annually, ~87 % wave approached from South-Southwest (SSW) quadrant at the breaker zone.

Wave period during pre-monsoon and post-monsoon varies in the range of 3.5 – 9.2 s and 3.2- 10.5 s respectively and during monsoon, the period varies in the range of 4- 9 s. The wave period values indicate that waves in the study areas are intermediate period waves as per the classification of Bromirski et al. (2005). Monthly averaged wave period is observed to be maximum (7.1 s) during July and minimum during February (5 s). Averaged values of wave period during pre-monsoon, post-monsoon and monsoon are 5.2, 5.8 and 6.5 s respectively. Similar variations in nearshore characteristics were observed by Glejin et al. (2015, 2013) and Arockiaraj et al. (2018) along Ratnagiri, 18 km south of the study region.

4.2 Long-term variations in nearshore characteristics

To determine the long-term variations in the breaking wave characteristics of the study region, monthly averaged values for each parameter were determined and long-term mean was computed. The long-term mean was subtracted from the monthly averaged time-series to estimate the variability of breaking parameters (Figure 5, a, b, c). Deviations from mean (DM) value of H_b , period and direction vary typically in the range of -0.35 to 0.4 m, -0.80 to 1 s and -16 to 12° respectively. Considerable interannual variations are observed in the breaker characteristics. Relatively larger breaker heights were observed during the year 2012 followed by 1994 and the lowest being observed during 2009 followed by 1993. Large breaker heights during 1994 (June) is due to the impact of a tropical cyclone over the Arabian Sea which was formed on June 5 and became a tropical cyclone on June 7 with an intensity of 100 km/h. The lower breaker heights during 2009 (June) is the response of delayed monsoon (Sanil Kumar and George, 2016). Peak values in the wave period were observed during 2004 followed by 1980 whereas, low values in wave period were observed during 1996 and 1986. In the case of mean wave directions, larger positive DM is observed during the year 2016 followed by the year 1985, indicating that more waves are approaching from the north. Negative DM values indicate that more waves approached from the south and are observed in its maximum during the year 1993 and 1994.

During 1979-2016, both H_b and direction show a negative trend ($-0.0001 \text{ m yr}^{-1}$ and $-0.04^\circ \text{ yr}^{-1}$) whereas, period shows a positive trend (0.08 s yr^{-1} , Figure 5, trend lines not shown) with a statistical significance of 95% confidence limit from the Mann Kendall Test. An annual averaged SWH and wave period at the offshore boundary and H_b is presented in Figure 6. Both SWH and period at the offshore boundary give a positive trend (trend lines not shown) of 0.0004 m yr^{-1}

(insignificant) and 0.0032 s yr^{-1} (90% confidence limit), whereas H_b shows a declining trend of $-0.0008 \text{ m yr}^{-1}$ with 90% confidence level. These negligible trends are due to the influence of intra-seasonal or intra-annual variations within a year which further leads to large biases in the long-term trend analysis. Thus a further investigation on monthly variations of breaker characteristics is carried out to understand more about its variations in a long-term period.

Figure 7 shows the long-term variations of the breaker height for different months. Except for January, June and December, all other months show a significant trend with 90% confidence limit. During the pre-monsoon months (FMAM), DM ranges in between -0.15 and 0.15 m and the trends are observed to be decreasing, with a maximum decrease observed during April ($-0.0051 \text{ m yr}^{-1}$) and minimum during May (-0.002 m yr^{-1}). The post-monsoon (ONDJ) also shows a significant decreasing trend with a maximum decline in the month of October ($-0.0023 \text{ m yr}^{-1}$) followed by November ($-0.0018 \text{ m yr}^{-1}$). DM values ranges in between -0.20 and 0.20 m during this period. During monsoon months, DM ranges in between -0.35 and 0.35 m and a significant increase in the H_b were observed during July (0.0029 m yr^{-1}) and September (0.0057 m yr^{-1}), but during August the trend shows a declining tendency ($-0.0026 \text{ m yr}^{-1}$). This weakening trend in wave heights during the month of August was previously reported by Shanas and Sanil Kumar (2014c) along the eastern Arabian Sea. Also, a statistically significant increasing trend (maximum $\sim 0.0020 \text{ m yr}^{-1}$) in wave heights was observed in the northern and southern regions of eastern Arabian Sea by Kumar and Anoop (2015). In a nutshell, along the breaker zones of Ganpatipule coast, breaker height shows a significant increasing trend during the monsoon season, whereas during non-monsoon the trend is decreasing.

Monthly variations in wave period for thirty-eight years is shown in Figure 8. The overall trend shows an increase in wave period for all the months except for November and December, which gives an insignificant negative trend. The DM value varies in the range of -0.8 to 0.8 s during all seasons. Pre-monsoon shows a positive trend with its peak during the month of May (0.023 s yr^{-1}) and minimum during February (0.015 s yr^{-1}). During monsoon, the overall trend is positive with a negligible and insignificant trend during the month of August. The maximum trend is observed during September (0.015 s yr^{-1}) and minimum during June (0.01 s yr^{-1}). DM values observed during post-monsoon months are negligible and are statistically insignificant too.

Figure 9 shows the monthly variations in wave direction at the breaker zone. Negative trends in the wave direction indicate the possibility of a shift in wave direction from mean averaged direction of a particular month to further south (anti-clockwise shift) and the positive trend indicates a shift towards further north (clockwise shift) from the mean direction. DM values vary in the range

of -16 to 16° during pre and post-monsoon, but during monsoon, the values range in between -3 and 8° . Pre-monsoon months show a significant negative trend with a maximum during March ($-0.19^\circ \text{ yr}^{-1}$) and minimum during February ($-0.11^\circ \text{ yr}^{-1}$). During April and May, the trend is the same ($-0.12^\circ \text{ yr}^{-1}$). For monsoon, insignificant trends are observed during July, August and September and significant but negligible ($-0.03^\circ \text{ yr}^{-1}$) trend during June. A significant negative trend is also observed during October ($-0.12^\circ \text{ yr}^{-1}$) whereas other months of the post-monsoon periods also show insignificant trends. As discussed in section 4.1, predominant wave directions during non-monsoon and monsoon months generally vary from 220 - 250° and the projected negative trends implies a southward shift in wave directions, stating there is no direction swing through the perpendicular (255°).

4.3 Littoral Drift

Using the CERC formula, LST rates at the Ganpatipule coast is estimated. Temporal variations in LST rates are observed during the study period (Figure 5, d). Anomaly values vary in the range of -2000 to 2000 m^3 . It is evident from the figure that LST rates are larger in the monsoon and comparatively lower during the non-monsoon period. Larger LST rates are observed during July for the year 2009, followed by 2006 and lower LST rates during 2009 (June) and 1987 (July). This intra-seasonal variation in LST during the year 2009 is the response of delayed monsoon (Sanil Kumar and George, 2016) which results in lower (larger) H_b during June (July) (Figure 7 f, g). Thus the wave breaking energy flux during the month of June was lower during 2009 giving low LST rates whereas, higher energy fluxes in the month of July which further leads to large LST rates.

Annual gross LST rate varies in the range 3.2 to $5 \times 10^5 \text{ m}^3 \text{ yr}^{-1}$ with an average value of $4.1 \times 10^5 \text{ m}^3 \text{ yr}^{-1}$ and annual net LST rate varies from 3.0 to $4.9 \times 10^5 \text{ m}^3 \text{ yr}^{-1}$ with an average value of $3.9 \times 10^5 \text{ m}^3 \text{ yr}^{-1}$. Comparison between measured LST (Sanil Kumar et al., 2003) with the present study gives a good agreement as discussed in section 2. Using time-series buoy data from Malpe and Kundapura, which is $\sim 400 \text{ km}$ south of the study region, Sanil Kumar et al. (2017) and Shanas and Sanil Kumar (2014a) estimated the annual gross LST as 3.5 and $3.3 \times 10^5 \text{ m}^3 \text{ yr}^{-1}$ respectively. Though during high sea states the wave conditions in central west coast India are similar due to the predominance of swells (Anoop et al., 2014), by comparison, a large difference ($\sim 90000 \text{ m}^3$) in LST rates (e.g., Sanil Kumar et al., 2017; Shanas and Sanil Kumar, 2014a) were observed with the present study. This is mainly due to the differences in shoreline orientation between the three study regions and biases with the modelled and measured data (see section 3). In the present study, an increase of 3 and 6° of incident wave direction for all the values in 2011 gives 24 and 48% increase in annual net LST rates and a decrease in 3 and 6° of incident wave direction gives a reduction in

annual net LST rates by 25 and 52% respectively. In the modelled data, up to 16% under prediction of SWH was observed when compared with the measured data (Figure 3). A 9 and 17% decrease in annual net LST rates were observed for a reduction of 5 and 10% of SWH in all the hourly data of 2011 respectively. A recent study by Chowdhury and Behera (2017) using ERA-I annual and monthly averaged wave parameters has estimated LST rates which vary in the range of 2 to $8 \times 10^5 \text{ m}^3 \text{ yr}^{-1}$ which is larger than reported in this study. This large difference between the present estimate of LST with Chowdhury and Behera (2017) is due to the fact that using the annual average value of wave parameters for LST estimate will lead to large error since the wave parameters show a large variation at shorter time span and also their study was based on data at offshore boundary point. Thus differences in shoreline orientation, source of wave data used in the model and the temporal resolution of the wave data time-series account to the differences in LST estimates between the present study and previously reported.

Due to the approach of waves from SSW quadrant, which is evident from Figure 4, a northerly net transport of LST is observed throughout the study period (Figure 10), since the direction of wave approach mainly determines the direction of LST. Annual net transport rates from 1979 to 2016 were also smoothed using a 5-year moving average filter, which helps in representing the impact of cumulative effects of prolonged events (Splinter et al., 2012). Considerable interannual variations in net LST is observed with larger net LST rates in the year 1994 followed by 2007, whereas lower net LST is observed during 1987 followed by 1983. An overall increasing trend in gross ($\sim 1596 \text{ m}^3 \text{ yr}^{-1}$, figure and trend line not shown) and net ($\sim 1840 \text{ m}^3 \text{ yr}^{-1}$) LST is observed with a 90% confidence interval. This is in contrary to the suggested declining trend by Chowdhury and Behera (2017), where they suggested a decline of LST rates induced by swells ($1240 \text{ m}^3 \text{ yr}^{-1}$) and wind-seas ($720 \text{ m}^3 \text{ yr}^{-1}$). This could be due to the use of largely biased monthly and annually averaged wave parameters for estimating LST, which fails to deliver more accurate estimations. Hence, for a realistic LST rate, wave data interval should be 6-h or less (Shanas and Sanil Kumar, 2014a).

The decade starting from 1979-1988 accounts for the least net LST rates with an average rate of $\sim 3.5 \times 10^5 \text{ m}^3 \text{ yr}^{-1}$. The decade from 1989-1998 and 1999-2008 accounts for $\sim 4.1 \times 10^5 \text{ m}^3 \text{ yr}^{-1}$ each and 2009-2016 accounts for $\sim 3.9 \times 10^5 \text{ m}^3 \text{ yr}^{-1}$. A declining trend (trend lines not shown) in the LST rates is observed in the decades 1979-1989 ($-5370 \text{ m}^3 \text{ yr}^{-1}$) and 2009-2016 ($-9607 \text{ m}^3 \text{ yr}^{-1}$) but are statistically insignificant. A decline in LST rates during 2009-2015 along the central west coast of India is also reported by Chowdhury and Behera (2017). A positive increase in LST rate is

observed from 1999 to 2009 ($3497 \text{ m}^3 \text{ yr}^{-1}$) and 1989-1999 ($3229 \text{ m}^3 \text{ yr}^{-1}$) decades, but significance (90%) is observed in the latter decade only.

Monthly variations in LST rates for different months is shown in Figure 11. During the pre-monsoon months (FMAM), a significant negative trend with 90% confidence limit is observed during April ($-3 \text{ m}^3 \text{ yr}^{-1}$) and insignificant trends are observed during other months. Though the trend values are larger during monsoon, only July ($22 \text{ m}^3 \text{ yr}^{-1}$) and September ($14 \text{ m}^3 \text{ yr}^{-1}$) show a significant increasing trend. However, they are significant with lower confidence (70%) limits during June ($17 \text{ m}^3 \text{ yr}^{-1}$) and August (negative trend, $-8 \text{ m}^3 \text{ yr}^{-1}$). During the post-monsoon months, all the trends are insignificant and negligible.

Since the model simulations allowed as to understand alongshore variations in the wave characteristics, the divergence of wave energy flux along the Ganpatipule coast was examined during the year 2011. The longshore component of wave power is computed for every hour during 2011 and monthly averaged value is shown in Figure 12. As expected low energy southward directed fluxes ($-0.1-0.3 \times 10^6 \text{ W/m}$) is observed during pre-monsoon due to the predominance of wind-seas from the northwest and low energy northward directed fluxes ($0.1-0.5 \times 10^6 \text{ W/m}$) during post-monsoon due to predominance of long-period swells from south and southwest. During monsoon with the presence of strong westerly waves, energy fluxes range from $0.5-1.5 \times 10^6 \text{ W/m}$. The study shows that the alongshore variation of the longshore component of wave power is minimum (0.4%) during monsoon and is maximum (27%) in April.

4.4 Regional climate influence

As discussed earlier, a predominance of both wind-seas and swells are observed in the study region during non-monsoon months, whereas, swell waves are predominant during monsoon. Wind-seas are locally generated, and swell waves, generated in the Indian Ocean sector and Somali coast travel larger distances from their zone of the generation before reaching the coast. High waves which are generated in the south Indian Ocean ($40-60^\circ \text{ S}$ and $20-40^\circ \text{ E}$) generally reaches the central west coast of Indian subcontinent within 5-6 days (Amrutha et al., 2017). Figure 13 (a, b, c) and 14 (a, b, c) show the maximum spatial correlation of wind fields and SWH with daily LST rates during the period from 1979-2016 along the North Indian Ocean for different seasons. The time lag (days) required to maximise the correlation coefficient for each grid cells is also shown in Figure 13(d, e, f) and Figure 14 (d, e, f). During FMAM, along northwestern and central Arabian Sea the maximum correlation between wind fields and LST generally ranges for 0.5-0.75 and 0.25-0.5 respectively within a time lag of 2 days. During JJAS, these correlations further become stronger and form a belt

from the equator to the south of Gulf of Oman which further extends to the west towards the Indian subcontinent. These positive correlations are associated with the monsoonal circulations or Findlater Jet (Findlater, 1969a; 1969b) which originates in the south Indian Ocean near Madagascar and emerges in the Arabian Sea and flows across the central parts to the west coast of India (Sanil Kumar and George, 2016). A strong correlation ($r > 0.75$) is observed in the belt at the central Arabian Sea ($65^{\circ}:70^{\circ}\text{E}$ and $15^{\circ}:20^{\circ}\text{N}$). Along these belts, the maximum correlations are observed within 1-3 day lag. During ONDJ, weak correlations ($r=0-0.25$) are observed in the Arabian Sea within a time lag of 6-8 days. The correlations between SWH and LST along northwestern and central Arabian Sea are observed to be stronger ($r > 0.75$) within a time lag of 2 days during FMAM and JJAS and it weakens towards the equator ($r= 0.5-0.75$). The strong wind field region along the central Arabian Sea during JJAS gives a strengthened positive correlation ($r > 0.75$) for SWH with the daily LST which implies that swells, as well as wind-seas, has a direct influence on this region during the monsoon and the wind-wave variabilities along this region could have a direct impact on the LST transports along the central west coast of India. During ONDJ these correlations are weaker ($r < 0.75$) in the Arabian Sea.

A detailed investigation of temporal variability of wind-wave climate across the highly correlated region ($65^{\circ}:70^{\circ}\text{E}$ and $15^{\circ}:20^{\circ}\text{N}$) in the central Arabian Sea region during monsoonal months has been carried out. Our analysis suggests a declining trend (Figure not shown) in wind speed for both June (-0.001 m yr^{-1}) and August (-0.015 m yr^{-1}) months whereas, an increasing trend during July (0.0025 m yr^{-1}) and September (0.032 cm yr^{-1}). However, a statistically significant trend is only observed during August and September (90%). The averaged wind speed during monsoon across this region shows an increasing (0.0066 m yr^{-1} , Figure 15) trend with a significance of 80%. SWH trends during June, July and September are 0.0089 , 0.01 , and 0.01 m yr^{-1} (Figure not shown) respectively and are observed to be increasing with 90% significance. During August, the trend is decreasing ($-0.0036 \text{ m yr}^{-1}$) with lower significance (80%). The averaged SWH during monsoon across this region suggests an increasing trend (0.0068 m yr^{-1} , Figure 15, significant at 99%). The observed increasing trends in LST rates (Figure 10) could be due to the increase in the wind-wave climate of this region. Thus, a region in the central Arabian Sea has been identified to have a potential influence on determining the LST rates at Ganpatipule coast, eastern Arabian Sea.

4.5 Impact of Pacific Climate variability on LST

To examine the inter-annual and decadal variability in estimated net LST, an Index from the net LST rates (Figure 10) has been created (Figure 16), expressed as deviations from the mean net transport rate, $\Delta Q = Q_{NET} - \overline{Q_{NET}}$, where $\overline{Q_{NET}}$ is the net mean transport over 38 years. An inverse relationship has been observed with net LST index and two significant modes of climate variability

in the tropical Pacific, ENSO and Pacific Decadal Oscillation (PDO). During the study period, the annual averaged Oceanic Niño Index (ONI) and net LST index (Figure 16, a) have a (80% confidence) weak negative correlation of 0.18 whereas a significant (90%) negative correlation of -0.29 is observed with a 5-yr smoothed (Figure 16, b) ONI index and LST rates. The major generating force of surface waves in the oceans are winds and the variabilities in wind anomalies caused by ENSO induce variations in wave climate (Schott et al., 2009). Thus peak El Niño (La Nina) events decrease (increase) winds in the equatorial Indian Ocean (Taschetto et al., 2011) which further leads to lower (higher) wave energy fluxes. During the past decades, very strong El Niño years ($ONI \geq 2.0$) are 1982-1983, 1997-1998 and 2015-2016 and moderate El Niño years ($ONI \sim 1.0$ to 1.5) are 1987-1988, 1991-1992, 1997-1998 and 2009-2010. Strong/moderate ($ONI \sim -1.0$ to -1.5) are observed during 1988-1989, 1999-2000, 2008-2009 and 2011-2012. In the present study, lower LST rates were not observed in the peak El Niño years but for a moderate El Niño year (1987, $\sim 3 \times 10^5 \text{ m}^3$). Strong/moderate El Niño (La Nina) years are generally associated with low (high) LST rates as compared with other years (Figure 16). However, the signatures of a large impact of ENSO alone on LST rates were not evident in the present study since there are fluctuations observed in the LST rates both in interannual and decadal timescales.

A strong negative correlation of 0.41 and 0.63 is observed with a confidence level of 90% between the annual averaged (Figure 16, a) and 5- yr smoothed (Figure 16, b) net LST Index and PDO. This indicates that PDO has an influence on LST rates both on interannual as well as decadal scales. Extreme phases of PDO are classified as warm and cool phases, and it waxes and wanes for every 15-25 years (Mantua and Hare, 2002) and their fluctuations in the strength of both phases occur in the ENSO frequency bands of 2 to 7 years (Minobe, 1999, 2000). According to Krishnamurthy and Krishnamurthy (2014), when the warm (cold) phase of PDO and El Niño (La-Niña) co-occurs, more intense droughts (floods) are likely to occur in the Indian peninsula. The hypothesis put forward by them explains the mechanism in which PDO affects the monsoon circulation. They suggest that trade winds are affected by the seasonal foot printing of SST from the North Pacific to the subtropical Pacific, which either strengthens or weakens the Walker circulation over the Pacific and Indian Oceans depending upon the phase of PDO. From 1977 to mid-1990, a warm PDO regime existed (MacDonald and Case, 2005; Mantua and Hare, 2002). As evident from the Figure 16 and section 4.3, lower LST rates during these decades are mainly due to warm phase in PDO which is further strengthened by the occurrence of one strong and two moderate El Niño events. However, the warm and cool phases of the PDO has been shortened in recent decades with a fluctuation span of 4-7 years. Since 2014, PDO shifted to the warm phase, which is associated with

the declining tendency of LST rates. Thus it is evident that Pacific climate variability has a direct impact on the LST along the eastern Arabian Sea both on interannual as well as decadal scales.

5 Conclusions

The study examined the long-term variations in nearshore wave characteristics and littoral drift at Ganpatipule coast, eastern Arabian Sea for 38 years (1979-2016). To the author's knowledge, this is the first analysis of long-term variations on nearshore parameters done along the eastern Arabian Sea using time-series data with 6-h interval. Statistical analysis suggests a good comparison with the measured and modelled wave parameters. Considerable annual variations in the breaker wave characteristics are observed. The breaker wave height generally varies in the range of 0.1 to 1.1 m during non-monsoon periods and 0.3 to 2.3 m during monsoon. The wave period varies in the range of 3.2 to 10.5 s during non-monsoon and 4-9 s during monsoon. Along the breaker zone, ~87% times the wave generally approaches from S-SW direction and predominant wave approaching direction are through 240-250°. For H_b , a decreasing trend is observed for pre and post-monsoon season with a maximum decline in the month of April and October respectively. Though a declining trend is observed in the month of August, the overall trend during the monsoon is positive, indicating the growing importance of the influence of monsoon on breaker heights in the coming decades. Significant positive trends in wave period are also observed during the pre-monsoon and monsoon. An anti-clockwise shift in wave direction is observed during the non-monsoon periods indicates the projected shifts do not swing through the perpendicular. During the monsoon, the directions are consistent.

Littoral drift rates along the study region are estimated using CERC and are in good agreement with previously reported rates along the central west coast of India. Annual gross LST rate varies in the range of 3.2 to $5 \times 10^5 \text{ m}^3 \text{ yr}^{-1}$ with an average value of $4.1 \times 10^5 \text{ m}^3 \text{ yr}^{-1}$. A northerly net transport is observed throughout the study period and it varies in the range of 3.0 to $4.9 \times 10^5 \text{ m}^3 \text{ yr}^{-1}$ with an average value of $3.9 \times 10^5 \text{ m}^3 \text{ yr}^{-1}$. This study also observed an increasing trend in the net transport rate with a rate of $1840 \text{ m}^3 \text{ yr}^{-1}$. LST rates at Ganpatipule coast in the eastern Arabian Sea is mainly influenced by the wind speed variabilities along the central Arabian Sea during the monsoon. Impact of Pacific climate variability on LST rates is observed during the first decade (1979-1989) which result in lower LST rates due to warm phase in PDO which is further strengthened by the occurrence of one strong and two moderate El Niño events.

The study provides a long-term perspective of LST variability along the eastern Arabian Sea for the first time, and the LST rate present in this paper is the maximum volume of sand which

moves along the shore for the hydrodynamic conditions present. However, there are certain uncertainties/limitations while estimating LST rates in this study, i.e., bathymetry along the study region is assumed to be unchanged during the simulation period, calibration of K coefficient on CERC formula is not dealt for all the months since the measured LST rates were available only from February to May and it gave good comparison with measured rates after using the correction factor and the wind input is not given to the wave transformation model. Even so, the associated results may be used as a basis for carrying out beach morphodynamic studies, long-term coastal behaviour and can also relate to shoreline changes in varying timescales along the study area.

Acknowledgements

The authors gratefully acknowledge the support of the Council of Scientific & Industrial Research, New Delhi to conduct this research. The ERA-I data used in this study are available from the ECMWF data server: <https://apps.ecmwf.int/datasets/data/interim-full-daily/levtype=sfc/>. The wave data used for the model validation are from the project funded by Ministry of Earth Sciences, New Delhi through Indian National Centre for Ocean Information Services, Hyderabad and is available on request for joint research work. Director, CSIR-NIO, Goa encouraged to carry out the study. We thank Jai Singh, Anoop and Glejin Johnson and Naseef Muhammad for the help provided during the data collection. We thank the three reviewers and the Editor for the suggestions which improved the scientific content of this paper. This work forms part of the Ph.D. thesis of the first author registered at Bharathidasan University and NIO contribution No. is -----.

References

- Adams, P. N., Inman, D. L., & Lovering, J. L. (2011). Effects of climate change and wave direction on longshore sediment transport patterns in Southern California. *Climatic Change*, *109*(1), 211–228. <https://doi.org/10.1007/s10584-011-0317-0>
- Amrutha, M. M., Kumar, V. S., & George, J. (2017). Observations of long-period waves in the nearshore waters of central west coast of India during the fall inter-monsoon period. *Ocean Engineering*, *131*, 244–262. <https://doi.org/10.1016/j.oceaneng.2017.01.014>
- Amrutha, M. M., Kumar, S., Bhaskaran, H., & Muhammed, N. (2019). Consistency of wave power at a location in the coastal waters of central eastern Arabian Sea. *Ocean Dynamics*, *69*(5), 543–560. doi : 10.1007/s10236-019-01267-1.
- Anoop, T. R., Sanil Kumar, V., & Shanas, P. R. (2014). Spatial and temporal variation of surface waves in shallow waters along the eastern Arabian Sea. *Ocean Engineering*, *81*, 150–15. <https://doi.org/10.1016/j.oceaneng.2014.02.010>
- Anoop, T. R., Kumar, V. S., Shanas, P. R., & Johnson, G. (2015). Surface wave climatology and its variability in the north Indian Ocean Based on ERA-interim reanalysis. *Journal of Atmospheric and Oceanic Technology*, *32*(7), 1372–1385. <https://doi.org/10.1175/JTECH-D-14-00212.1>

- Anoop, T. R., Sanil Kumar, V., Shanas, P. R., Glejin, J., & Amrutha, M. M. (2016). Indian Ocean Dipole modulated wave climate of eastern Arabian Sea. *Ocean Science*, *12*(2), 369–378. <https://doi.org/10.5194/os-12-369-2016>
- Arockiaraj, S., Kankara, R. S., DoraS., G. U., & S. Sathish. (2018). Estimation of seasonal morpho-sedimentary changes at headland bound and exposed beaches along south Maharashtra, west coast of India. *Environmental Earth Sciences*, *77*(17), 1–16. <https://doi.org/10.1007/s12665-018-7790-y>
- Battjes, J. A., & Stive, M. J. F. (1985). Calibration and verification of a dissipation model for random breaking waves. *Journal of Geophysical Research: Oceans*, *90*(C5), 9159–9167.
- Booij, N., Ris, R. R. C., & Holthuijsen, L. H. L. (1999). A third-generation wave model for coastal regions 1. Model description and validation. *Journal of Geophysical Research*, *104*(C4), 7649–7666. <https://doi.org/10.1029/98jc02622>
- Bromirski, P. D., Cayan, D. R., & Flick, R. E. (2005). Wave spectral energy variability in the northeast Pacific. *Journal of Geophysical Research C: Oceans*, *110*(C3). <https://doi.org/10.1029/2004JC002398>
- Casas-Prat, M., & Sierra, J. P. (2012). Trend analysis of wave direction and associated impacts on the Catalan coast. *Climatic Change*, *115*(3–4), 667–691. <https://doi.org/10.1007/s10584-012-0466-9>
- Casas-Prat, Mercè, McInnes, K. L., Hemer, M. A., & Sierra, J. P. (2016). Future wave-driven coastal sediment transport along the Catalan coast (NW Mediterranean). *Regional Environmental Change*, *16*(6), 1739–1750. <https://doi.org/10.1007/s10113-015-0923-x>
- CERC. (1984). *Shore Protection Manual. Vols I and II. Coastal Engineering Research Center. U.S. Army Corps of Engineers, Washington, DC. U.S. Government Printing Office, Vicksburg.*
- Chini, N., Stansby, P., Leake, J., Wolf, J., Roberts-Jones, J., & Lowe, J. (2010). The impact of sea level rise and climate change on inshore wave climate: A case study for East Anglia (UK). *Coastal Engineering*, *57*(11–12), 973–984. <https://doi.org/10.1016/j.coastaleng.2010.05.009>
- Chowdhury, P., & Behera, M. R. (2017). Effect of long-term wave climate variability on longshore sediment transport along regional coastlines. *Progress in Oceanography*, *156*, 145–153. <https://doi.org/10.1016/j.pocean.2017.06.001>
- Dee, D. P., Uppala, S. M., Simmons, A. J., Berrisford, P., Poli, P., Kobayashi, S., et al. (2011). The ERA-Interim reanalysis: Configuration and performance of the data assimilation system. *Quarterly Journal of the Royal Meteorological Society*, *137*(656), 553–597. <https://doi.org/10.1002/qj.828>
- Dodet, G., Bertin, X., & Taborda, R. (2010). Wave climate variability in the North-East Atlantic Ocean over the last six decades. *Ocean Modelling*, *31*(3–4), 120–131. <https://doi.org/10.1016/j.ocemod.2009.10.010>
- Du, Y., Xie, S. P., Huang, G., & Hu, K. (2009). Role of air-sea interaction in the long persistence of El Niño-induced north Indian Ocean warming. *Journal of Climate*, *22*(8), 2023–2038. <https://doi.org/10.1175/2008JCLI2590.1>

- Eldeberky, Y. (1997). Nonlinear transformation of wave spectra in the nearshore zone. *Oceanographic Literature Review*, 4(44), 297.
- Findlater, J. (1969a). A major low level air current near the Indian Ocean during the northern summer. *Quarterly Journal of the Royal Meteorological Society*, 95(404), 362–380. <https://doi.org/10.1002/qj.49709540409>
- Findlater, J. (1969b). Interhemispheric transport of air in the lower troposphere over the western Indian Ocean. *J. R. Met. Soc.*, 95(404), 400–403. <https://doi.org/10.1002/qj.49709540412>
- Gallagher, S., Tiron, R., & Dias, F. (2014). A long-term nearshore wave hindcast for Ireland: Atlantic and Irish sea coasts (1979-2012). *Ocean Dynamics*, 64(8), 1163–1180. <https://doi.org/10.1007/s10236-014-0728-3>
- Glejin, J., Sanil Kumar, V., Balakrishnan Nair, T. M., & Singh, J. (2013). Influence of winds on temporally varying short and long period gravity waves in the near shore regions of the eastern Arabian Sea. *Ocean Science*, 9(2), 343–353. <https://doi.org/10.5194/os-9-343-2013>
- Glejin, Johnson, Kumar, V. S., & Singh, J. (2015). Inter-annual Variations in Wave Characteristics off Ratnagiri, Northeast Arabian Sea. *Aquatic Procedia*, 4, 25–31. <https://doi.org/10.1016/j.aqpro.2015.02.005>
- Harley, M. D., Turner, I. L., Short, A. D., & Ranasinghe, R. (2010). Interannual variability and controls of the Sydney wave climate. *International Journal of Climatology*, 30(9), 1322–1335. <https://doi.org/10.1002/joc.1962>
- Hasselmann, K., Barnett, T. P., Bouws, E., Carlson, H., Cartwright, D. E., Enke, K., et al. (1973). Measurements of Wind-Wave Growth and Swell Decay during the Joint North Sea Wave Project (JONSWAP). *Ergänzungsheft Zur Deutschen Hydrographischen Zeitschrift Reihe*, 8–12. <https://doi.org/citeulike-article-id:2710264>
- Hemer, M. A., Church, J. A., & Hunter, J. R. (2010). Variability and trends in the directional wave climate of the Southern Hemisphere. *International Journal of Climatology*, 30(4), 475–491. <https://doi.org/10.1002/joc.1900>
- Hydraulics, W. L. D. (2006). *Delft3D User Manual*.
- IPCC. (2013). Climate change 2013: The physical science basis-conclusions. *Bulletin Fuer Angewandte Geologie*. <https://doi.org/10.5169/seals-391142>
- Izaguirre, C., Mendez, F. J., Menendez, M., Luceño, A., & Losada, I. J. (2010). Extreme wave climate variability in southern Europe using satellite data. *Journal of Geophysical Research: Oceans*, 115(C4). <https://doi.org/10.1029/2009JC005802>, 2010
- Izaguirre, C., Méndez, F. J., Menéndez, M., & Losada, I. J. (2011). Global extreme wave height variability based on satellite data. *Geophysical Research Letters*, 38(10). <https://doi.org/10.1029/2011GL047302>
- Kamphuis, J. W. (2000). *Introduction to Coastal Engineering and Management. Advanced Series on Ocean Engineering*. <https://doi.org/10.1007/s13398-014-0173-7.2>

- Kamphuis, J. W. (2002). Alongshore transport of sand. In *Proc. 28 Coastal Engineering Conference, ASCE* (pp. 2478–2490.).
- Klein, S. A., Soden, B. J., & Lau, N. C. (1999). Remote sea surface temperature variations during ENSO: Evidence for a tropical atmospheric bridge. *Journal of Climate*, *12*(4), 917–932. [https://doi.org/10.1175/1520-0442\(1999\)012<0917:RSSTVD>2.0.CO;2](https://doi.org/10.1175/1520-0442(1999)012<0917:RSSTVD>2.0.CO;2)
- Krishnamurthy, L., & Krishnamurthy, V. (2014). Influence of PDO on South Asian summer monsoon and monsoon-ENSO relation. *Climate Dynamics*, *42*(9–10), 2397–2410. <https://doi.org/10.1007/s00382-013-1856-z>
- Krishnan, R., & Sugi, M. (2003). Pacific decadal oscillation and variability of the Indian summer monsoon rainfall. *Climate Dynamics*, *21*(3–4), 233–242. <https://doi.org/10.1007/s00382-003-0330-8>
- Kumar, P., Min, S. K., Weller, E., Lee, H., & Wang, X. L. (2016). Influence of climate variability on extreme ocean surface wave heights assessed from ERA-interim and ERA-20C. *Journal of Climate*, *29*(11), 4031–4046. <https://doi.org/10.1175/JCLI-D-15-0580.1>
- Kumar, V. Sanil, & Anoop, T. R. (2015). Spatial and temporal variations of wave height in shelf seas around India. *Natural Hazards*, *78*(3), 1693–1706. <https://doi.org/10.1007/s11069-015-1796-5>
- Kumar, V. Sanil, & Naseef, T. M. (2015). Performance of ERA-interim wave data in the nearshore waters around India. *Journal of Atmospheric and Oceanic Technology*, *32*(6), 1257–1269. <https://doi.org/10.1175/JTECH-D-14-00153.1>
- Kumar, V S, Anand, N. M., Ashok, K., & Mandal, S. (2014). Multi peakedness and Groupiness of Shallow Water Waves Along Indian Coast. *Journal of Coastal Research*, *19*(4), 1052–1065.
- MacDonald, G. M., & Case, R. A. (2005). Variations in the Pacific Decadal Oscillation over the past millennium. *Geophysical Research Letters*. <https://doi.org/10.1029/2005GL022478>
- Mantua, N. J., & Hare, S. R. (2002). The Pacific Decadal Oscillation. *Journal of Oceanography*. <https://doi.org/10.1023/A:1015820616384>
- Mantua, N. J., Hare, S. R., Zhang, Y., Wallace, J. M., & Francis, R. C. (1997). A Pacific Interdecadal Climate Oscillation with Impacts on Salmon Production. *Bulletin of the American Meteorological Society*, *78*(6), 1069–1080. [https://doi.org/10.1175/1520-0477\(1997\)078<1069:APICOW>2.0.CO;2](https://doi.org/10.1175/1520-0477(1997)078<1069:APICOW>2.0.CO;2)
- Minobe, S. (1999). Resonance in bidecadal and pentadecadal climate oscillations over the North Pacific: Role in climatic regime shifts. *Geophysical Research Letters*. <https://doi.org/10.1029/1999GL900119>
- Minobe, S. (2000). Spatio-temporal structure of the pentadecadal variability over the North Pacific. *Progress in Oceanography*. [https://doi.org/10.1016/S0079-6611\(00\)00042-2](https://doi.org/10.1016/S0079-6611(00)00042-2)
- Mortlock, T. R., Goodwin, I. D., & Turner, I. L. (2014). Nearshore SWAN model sensitivities to measured and modelled offshore wave scenarios at an embayed beach compartment, NSW, Australia. *Australian Journal of Civil Engineering*, *12*(1), 67–82. <https://doi.org/10.7158/C14-016.2014.12.1>

- National Hydrographic Office; Dehradun; India. (2004). *West Coast, Maharashtra Coast. Approaches to Ratnagiri, Hydrographic chart no 2028.*
- Newman, M., Compo, G. P., & Alexander, M. A. (2003). ENSO-forced variability of the Pacific decadal oscillation. *Journal of Climate*, 16(23), 3853–3857. [https://doi.org/10.1175/1520-0442\(2003\)016<3853:EVOTPD>2.0.CO;2](https://doi.org/10.1175/1520-0442(2003)016<3853:EVOTPD>2.0.CO;2)
- Newman, M., Alexander, M. A., Ault, T. R., Cobb, K. M., Deser, C., Di Lorenzo, E., et al. (2016). The Pacific decadal oscillation, revisited. *Journal of Climate*, 29(12), 4399–4427. <https://doi.org/10.1175/JCLI-D-15-0508.1>
- Van Rijn, L. C. (2014). A simple general expression for longshore transport of sand, gravel and shingle. *Coastal Engineering*, 90, 23–39. <https://doi.org/10.1016/j.coastaleng.2014.04.008>
- Rogers, W. E., Kaihatu, J. M., Hsu, L., Jensen, R. E., Dykes, J. D., & Holland, K. T. (2007). Forecasting and hindcasting waves with the SWAN model in the Southern California Bight. *Coastal Engineering*, 54(1), 1–15. <https://doi.org/10.1016/j.coastaleng.2006.06.011>
- Sanil Kumar, V., & George, J. (2016). Influence of Indian summer monsoon variability on the surface waves in the coastal regions of eastern Arabian Sea. *Annales Geophysicae*, 34, 871–885. <https://doi.org/10.5194/angeo-34-871-2016>
- Sanil Kumar, V., Anand, N. M., Chandramohan, P., & Naik, G. N. (2003). Longshore sediment transport rate - Measurement and estimation, central west coast of India. *Coastal Engineering*, 48(2), 95–109. [https://doi.org/10.1016/S0378-3839\(02\)00172-2](https://doi.org/10.1016/S0378-3839(02)00172-2)
- Sanil Kumar, V., Johnson, G., Udhaba Dora, G., Chempalayil, S. P., Singh, J., & Pednekar, P. (2012). Variations in nearshore waves along Karnataka, west coast of India. *Journal of Earth System Science*, 121(2), 393–403. <https://doi.org/10.1007/s12040-012-0160-3>
- Sanil Kumar, V., Shanas, P. R., Dora, G. U., Glejin, J., & Philip, S. (2017). Longshore sediment transport in the surf zone based on different formulae: a case study along the central west coast of India. *Journal of Coastal Conservation*, 21(1), 1–13. <https://doi.org/10.1007/s11852-016-0462-8>
- Schott, F. A., Xie, S. P., & McCreary, J. P. (2009). Indian ocean circulation and climate variability. *Reviews of Geophysics*. <https://doi.org/10.1029/2007RG000245>
- Semedo, A., Sušelj, K., Rutgersson, A., & Sterl, A. (2011). A global view on the wind sea and swell climate and variability from ERA-40. *Journal of Climate*, 24(5), 1461–1479. <https://doi.org/10.1175/2010JCLI3718.1>
- Shanas, & Sanil Kumar, V. (2014a). Coastal processes and longshore sediment transport along Kundapura coast, central west coast of India. *Geomorphology*, 214, 436–451. <https://doi.org/10.1016/j.geomorph.2014.02.027>
- Shanas, P. R., & Sanil Kumar, V. (2014b). Comparison of ERA-Interim waves with buoy data in the eastern Arabian Sea during high waves. *Indian Journal of Marine Sciences*, 43(7).
- Shanas, P. R., & Sanil Kumar, V. (2014c). Temporal variations in the wind and wave climate at a location in the eastern Arabian Sea based on ERA-Interim reanalysis data. *Natural Hazards and Earth System Sciences*, 14(5). <https://doi.org/10.5194/nhess-14-1371-2014>

- Sharma, S., Kumar, V. S., & Gowthaman, R. (2017). Textural characteristics and morphosedimentary environment of foreshore zone along Ganpatipule, Maharashtra, India. *Marine Georesources and Geotechnology*, 35(6), 887–894. <https://doi.org/10.1080/1064119X.2016.1259697>
- Shimura, T., Mori, N., & Mase, H. (2013). Ocean waves and teleconnection patterns in the northern hemisphere. *Journal of Climate*, 26(21), 8654–8670. <https://doi.org/10.1175/JCLI-D-12-00397.1>
- Short, A. D. (2012). Coastal processes and beaches. *Nature Education Knowledge*, 3(10), 15.
- Silva, A. N., Taborda, R., Bertin, X., & Dodet, G. (2012). Seasonal to Decadal Variability of Longshore Sand Transport at the Northwest Coast of Portugal. *Journal of Waterway, Port, Coastal, and Ocean Engineering*, 138(6), 464–472. [https://doi.org/10.1061/\(asce\)ww.1943-5460.0000152](https://doi.org/10.1061/(asce)ww.1943-5460.0000152)
- Splinter, K. D., Davidson, M. A., Golshani, A., & Tomlinson, R. (2012). Climate controls on longshore sediment transport. *Continental Shelf Research*, 48, 146–156. <https://doi.org/10.1016/j.matlet.2015.12.057>
- Taschetto, A. S., Gupta, A. Sen, Hendon, H. H., Ummenhofer, C. C., & England, M. H. (2011). The contribution of Indian Ocean sea surface temperature anomalies on Australian summer rainfall during EL Niño events. *Journal of Climate*. <https://doi.org/10.1175/2011JCLI3885.1>
- Thom, B. G., & Hall, W. (1991). Behaviour of beach profiles during accretion and erosion dominated periods. *Earth Surface Processes and Landforms*, 16(2), 113–127. <https://doi.org/10.1002/esp.3290160203>
- Toimil, A., Losada, I. J., Camus, P., & Díaz-Simal, P. (2017). Managing coastal erosion under climate change at the regional scale. *Coastal Engineering*, 128, 106–122. <https://doi.org/10.1016/j.coastaleng.2017.08.004>
- Vledder, G. Van, Zijlema, M., & Holthuijsen, L. (2012). REVISITING THE JONSWAP BOTTOM FRICTION FORMULATION. *Coastal Engineering Proceedings*, 1(32), 41. <https://doi.org/10.9753/icce.v32.waves.41>
- Wandres, M., Pattiaratchi, C., Hetzel, Y., & Wijeratne, E. M. S. (2018). The response of the southwest Western Australian wave climate to Indian Ocean climate variability. *Climate Dynamics*, 50(5–6), 1533–1557. <https://doi.org/10.1007/s00382-017-3704-z>
- Webster, P. J., & Yang, S. (1992). Monsoon and Enso: Selectively Interactive Systems. *Quarterly Journal of the Royal Meteorological Society*, 118(507), 877–926. <https://doi.org/10.1002/qj.49711850705>
- Weisse, R., & Günther, H. (2007). Wave climate and long-term changes for the Southern North Sea obtained from a high-resolution hindcast 1958-2002. *Ocean Dynamics*, 57(3), 161–172. <https://doi.org/10.1007/s10236-006-0094-x>
- Wyrtki, K. (1981). An Estimate of Equatorial Upwelling in the Pacific. *Journal of Physical Oceanography*, 11(9), 1205–1214. [https://doi.org/10.1175/1520-0485\(1981\)011<1205:AEOEUI>2.0.CO;2](https://doi.org/10.1175/1520-0485(1981)011<1205:AEOEUI>2.0.CO;2)

Table 1: Bias in different wave parameters estimated using model with measured data in different seasons of 2011 and 2012

Wave parameters	2011			2012		
	FMAM	JJAS	ONDJ	FMAM	JJAS	ONDJ
Significant wave height (m)	-0.17	-0.35	-0.06	-0.16	-0.31	0.007
Mean wave period (s)	0.34	0.26	0.80	0.64	0.24	1.14
Mean wave direction (Deg)	-2	-5	-23	-0.5	-6	-17

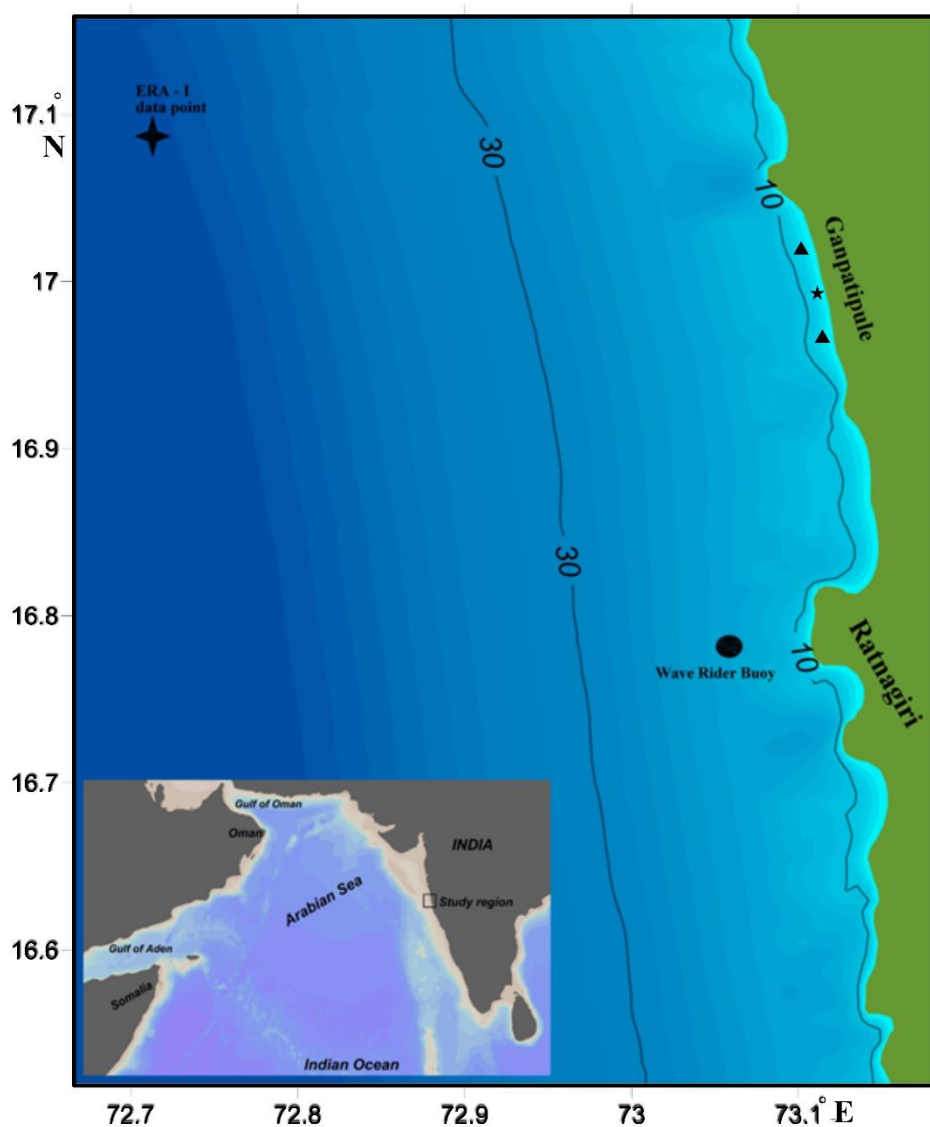


Figure 1. The study region in the Arabian Sea is shown in the inside figure. The outer figure is the bathymetry interpolated study domain used in the wave transformation model with lateral boundaries along north and south and the open boundary to the west. The location of wave rider buoy, ERA- I data point and the point (star) where the transformed wave data is extracted is also shown. The depth contours are in meters (m). The points considered for alongshore variation of wave power is also shown (triangle)

(a) significant wave height (m); (b) peak wave period (s); (c) swell (%); (d) wind-sea (%); (e) ERA-Interim wave height

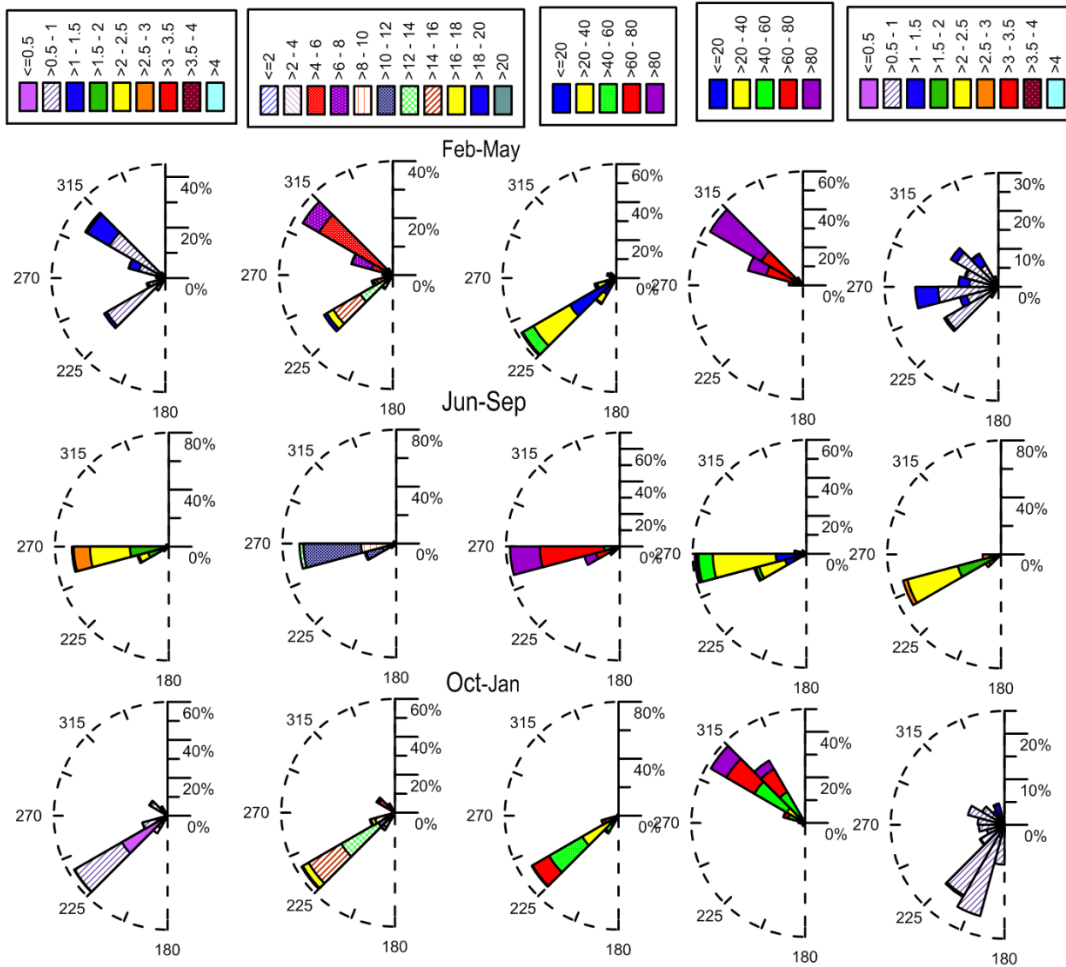


Figure 2. Wave roses during different seasons of 2012. Top panel is for February-May, middle panel is for June-September and bottom panel is for October-January. (a) significant wave height and mean wave direction, (b) peak wave period and mean wave direction, (c) percentage of swell in the measured data and mean wave direction, (d) percentage of wind-sea in the measured data and mean wave direction, (e) significant wave height and mean wave direction of ERA- Interim data. The radius of the figure indicates the percentage of the time

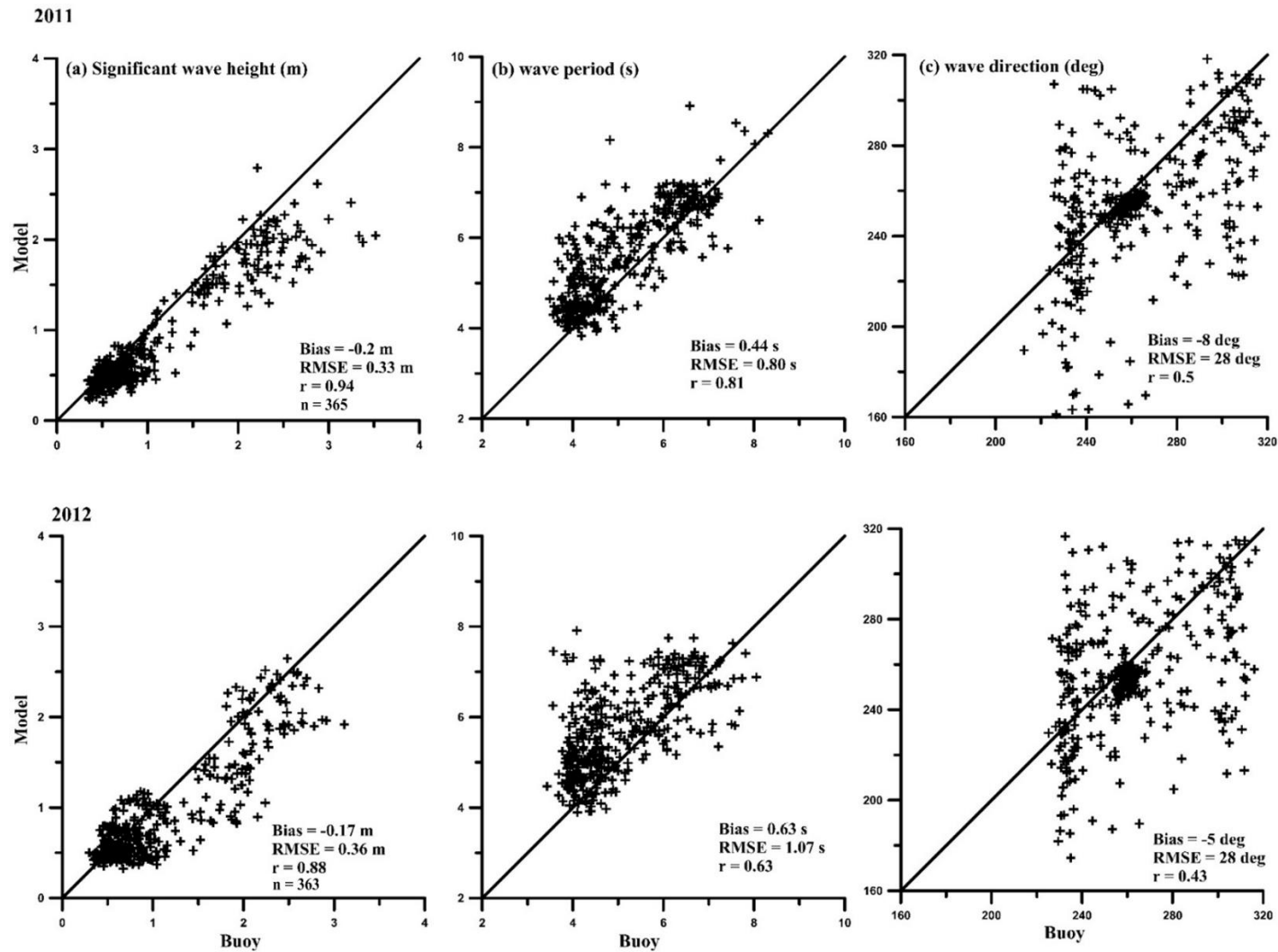


Figure 3. Scatter plot of daily averaged (a) significant wave height, (b) wave period and (c) wave direction between model simulation and buoy data for 2011 and 2012

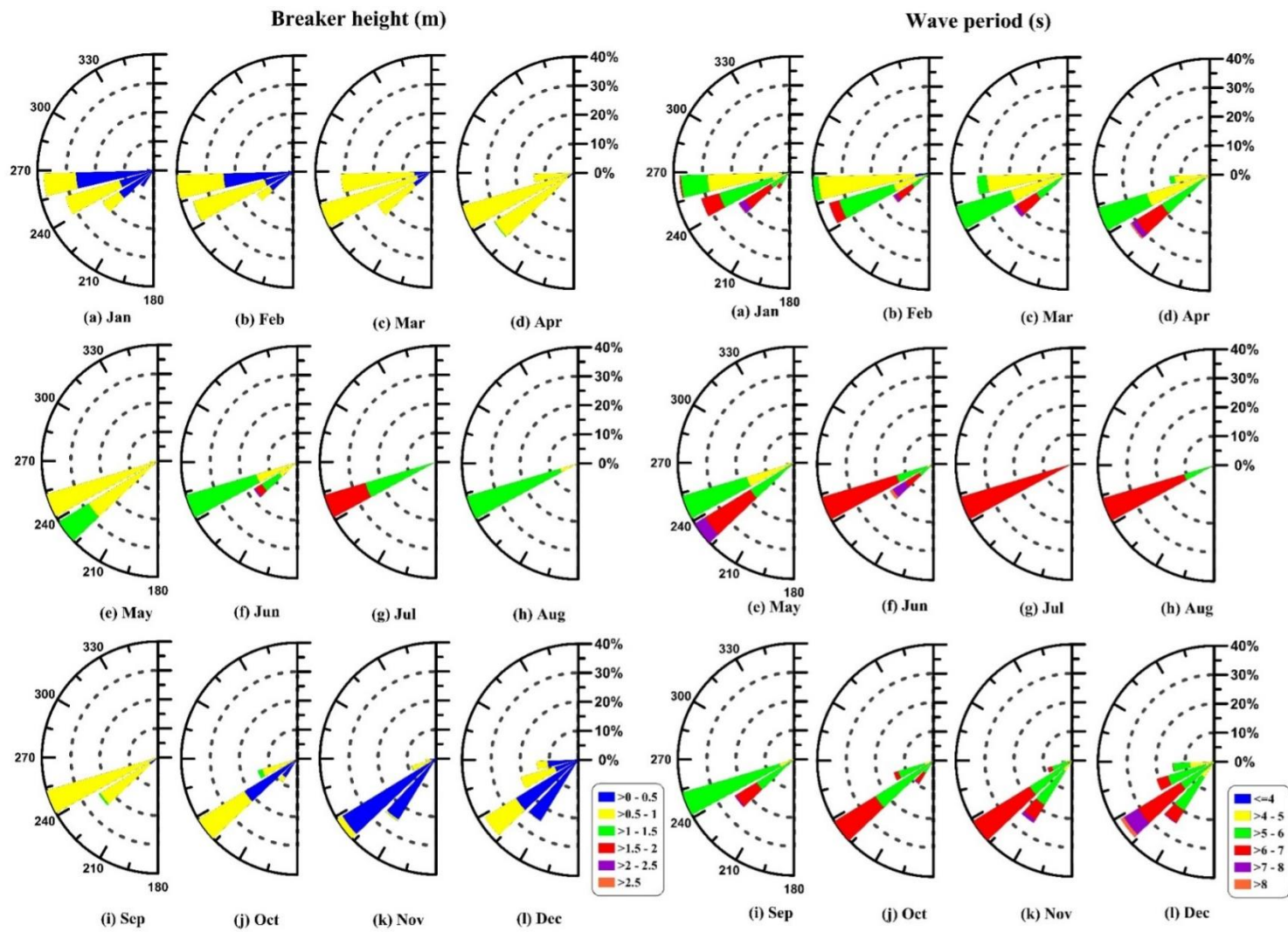


Figure 4. Wave rose diagram based on breaker height and wave period from 1979 – 2016

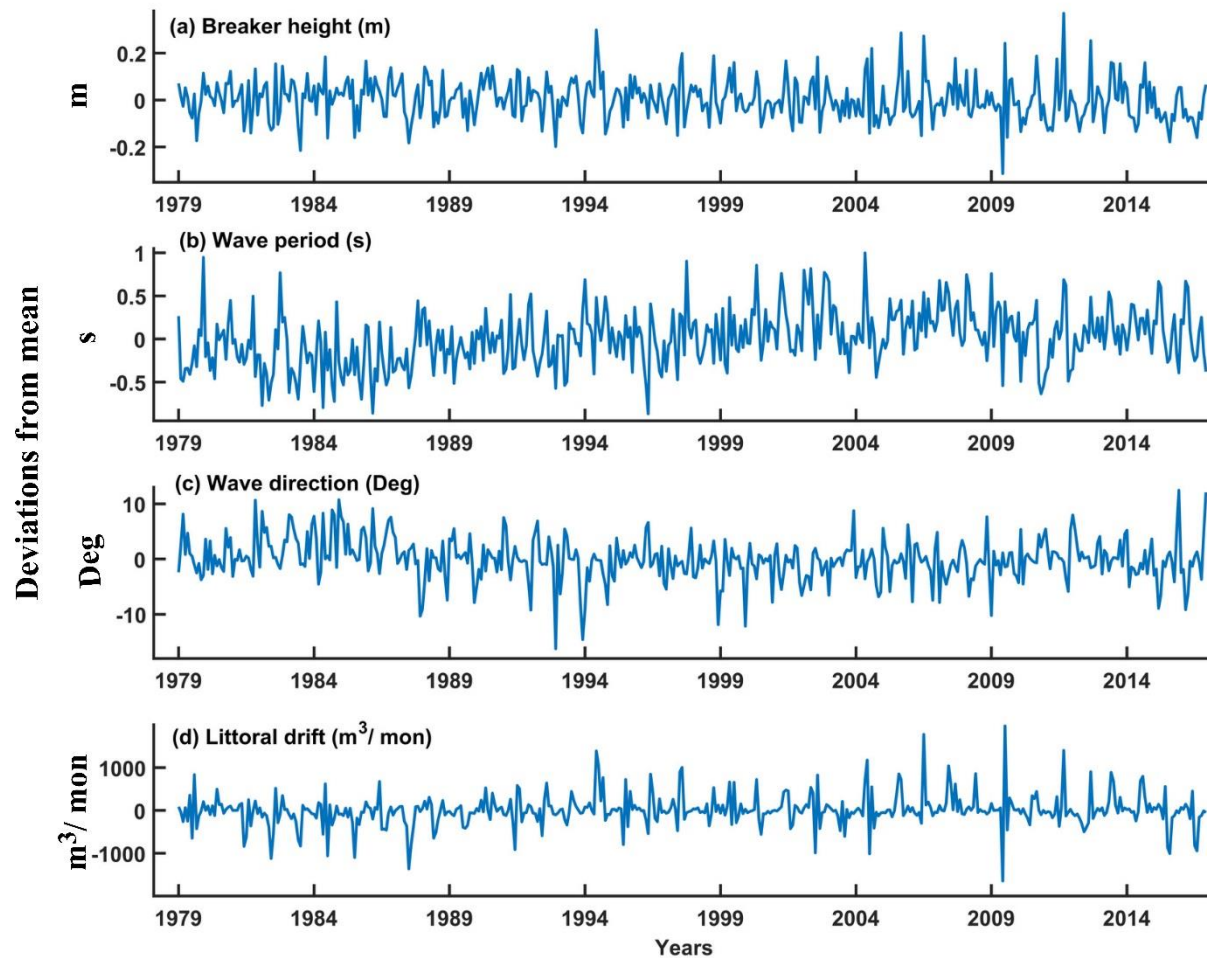


Figure 5. Monthly averaged deviations from the mean for a) breaker height (m) , b) wave period (s) , c) wave direction (Deg) and d) littoral drift (m³/mon) during 1979 to 2016

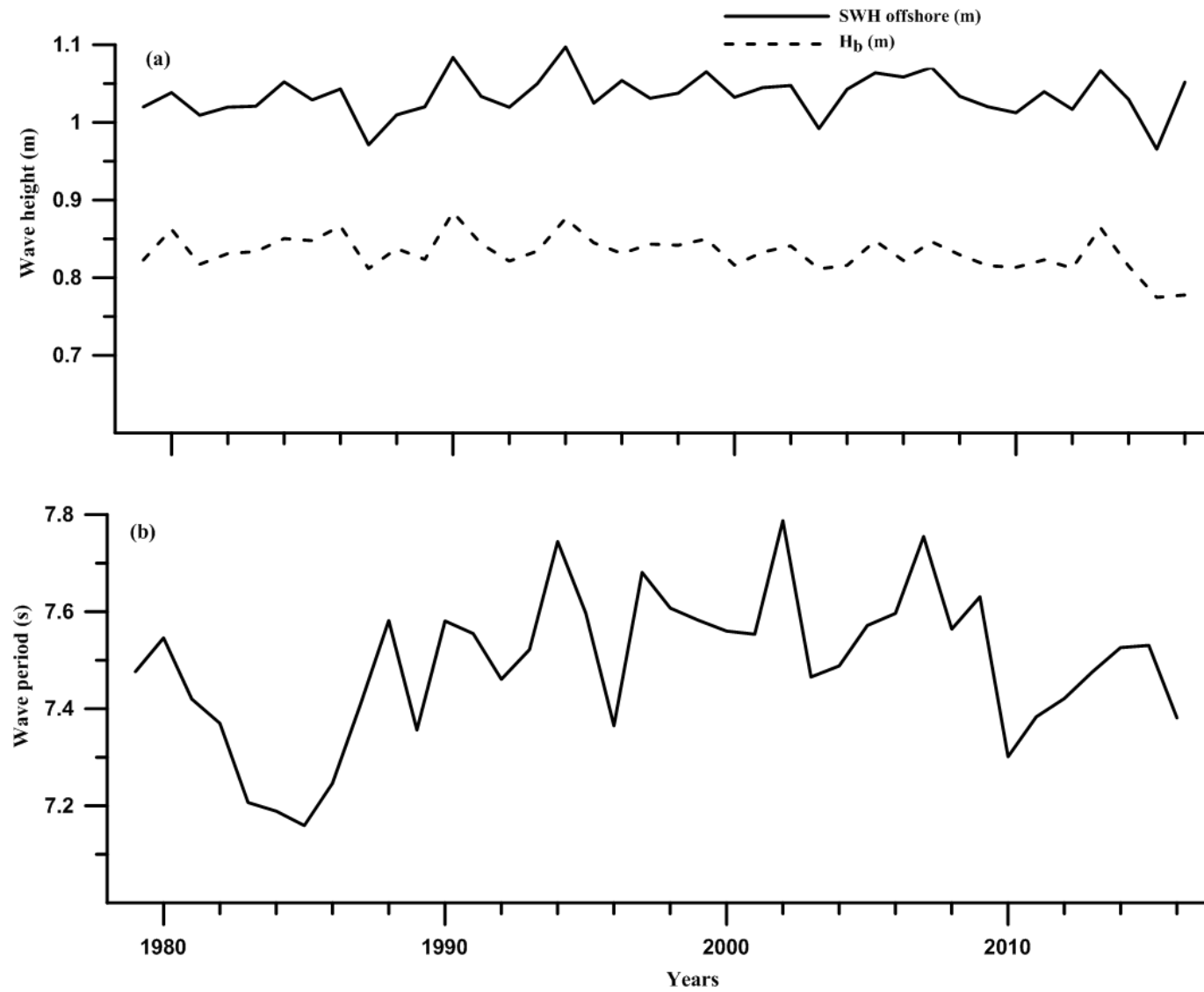


Figure 6. Annual averaged (a) wave height at the offshore boundary and breaker zone and (b) mean wave period at the offshore boundary

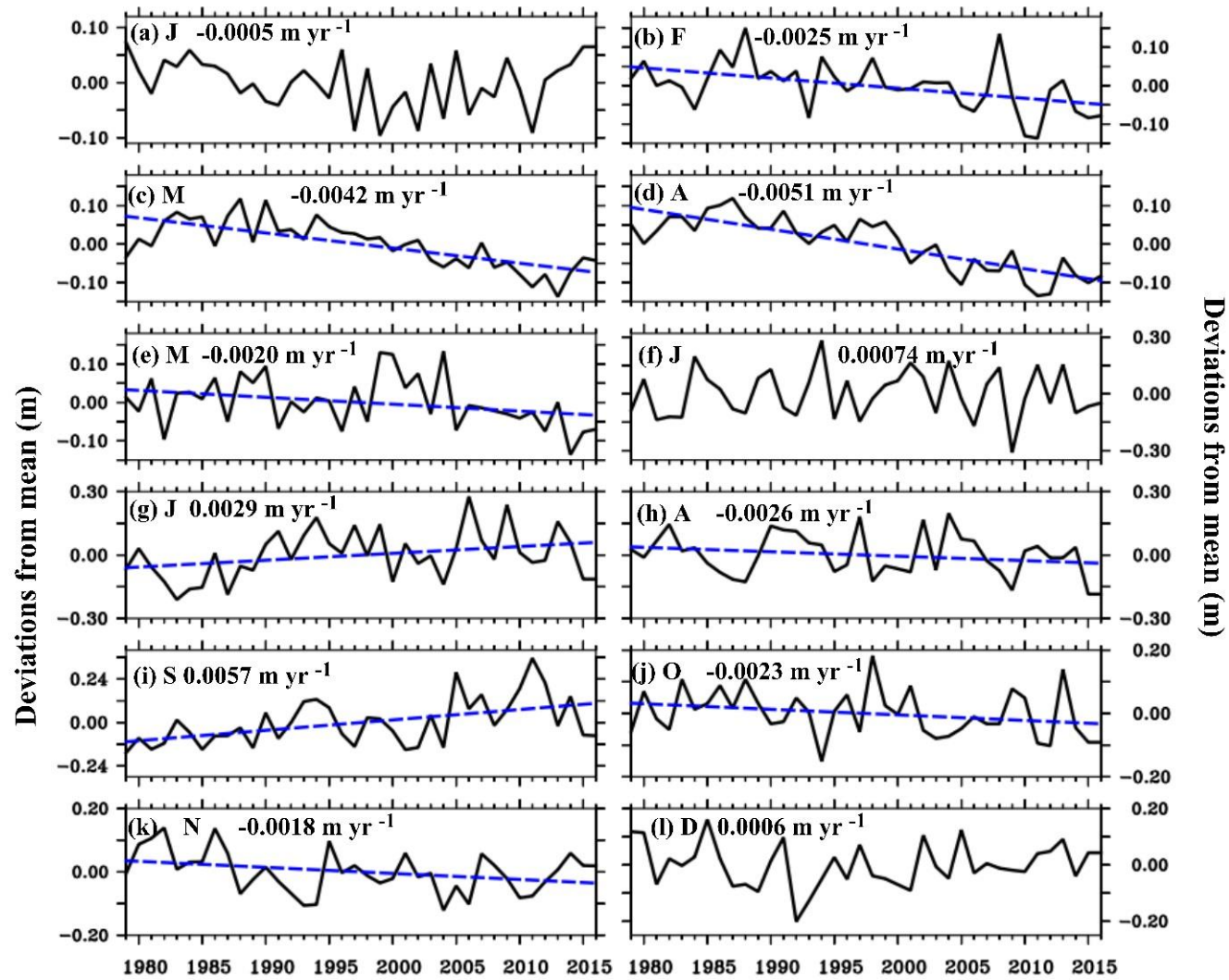


Figure 7. Monthly variations in deviations from mean of breaker wave height (m). Trend lines significant at 90% confidence interval are shown.

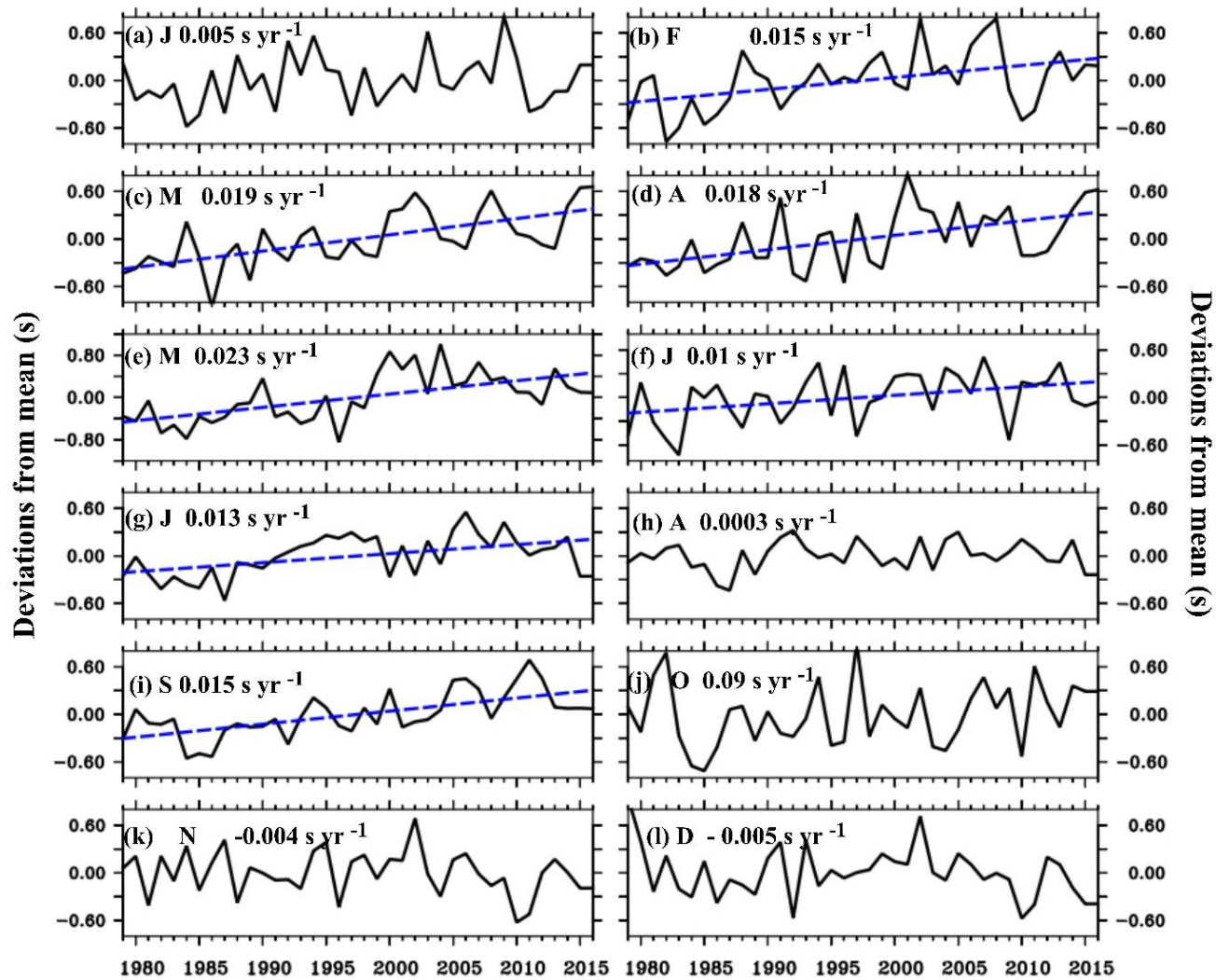


Figure 8. Monthly variations in deviations from mean of wave period (s). Trend lines significant at 90% confidence interval are shown.

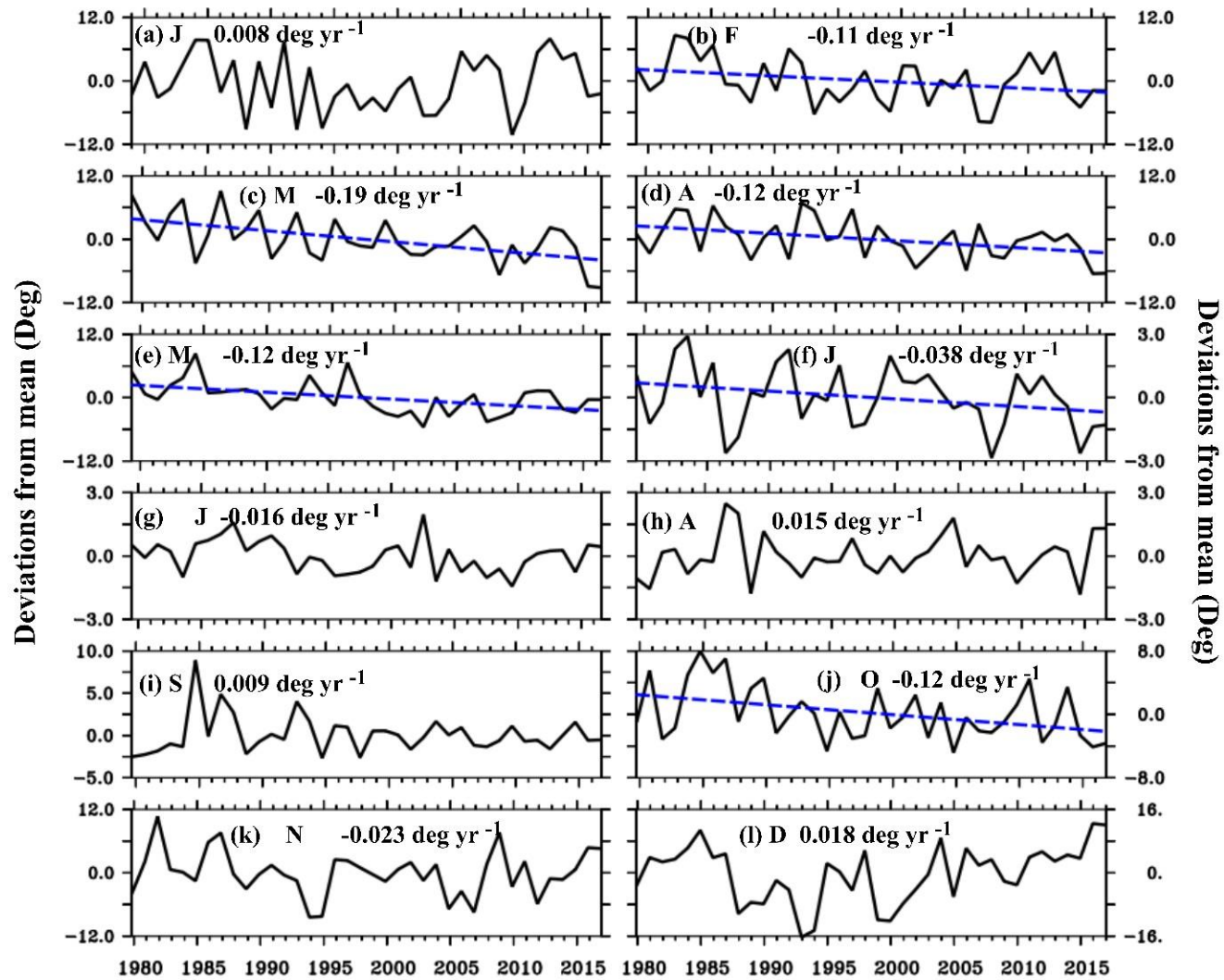


Figure 9. Monthly variations in deviations from mean of wave direction (Deg). Trend lines significant at 90% confidence interval are shown.

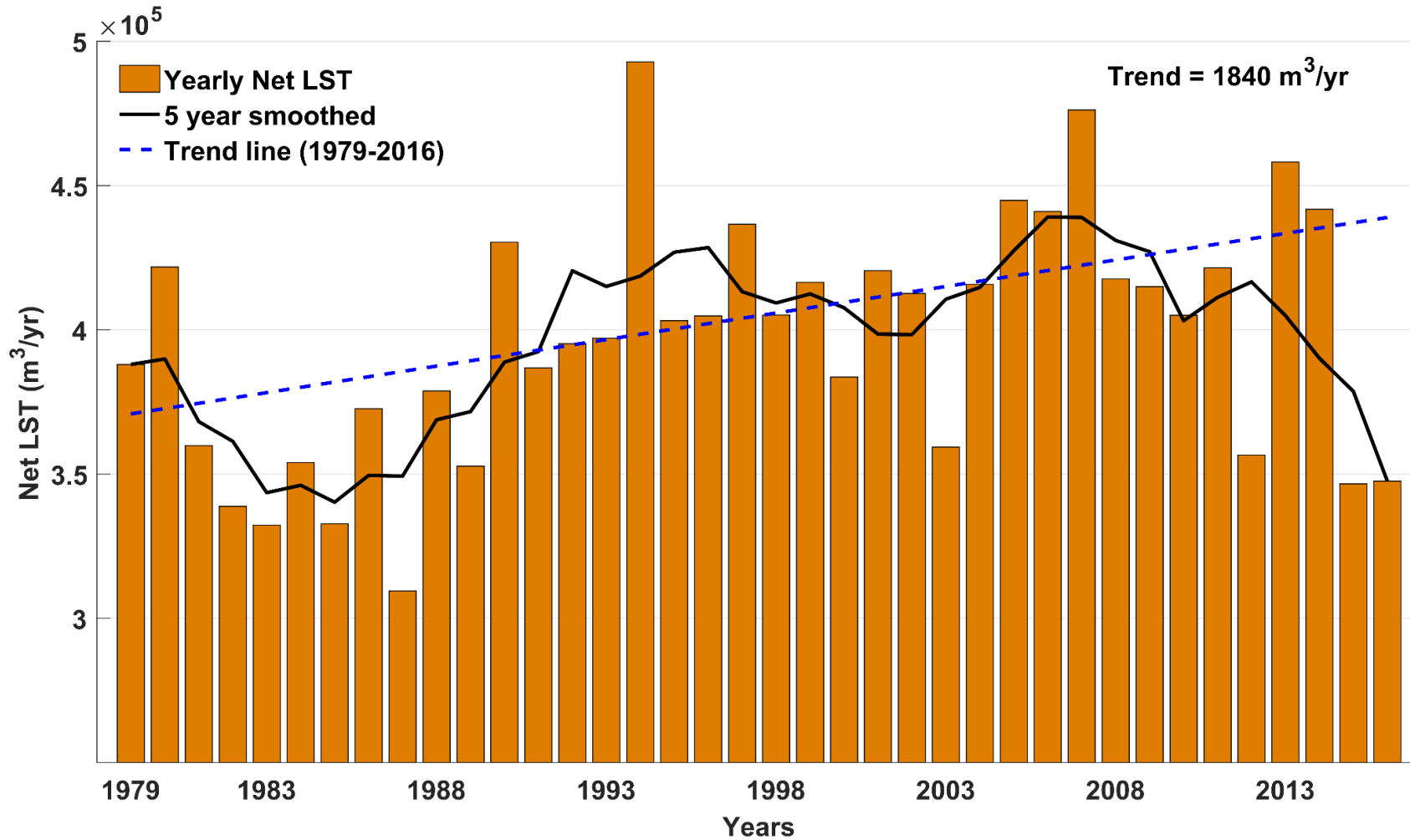


Figure 10. Yearly net longshore sediment transport (LST) estimates during 1979- 2016. Solid bar represents the net yearly transport, while thin line represents the 5 year smoothed values.

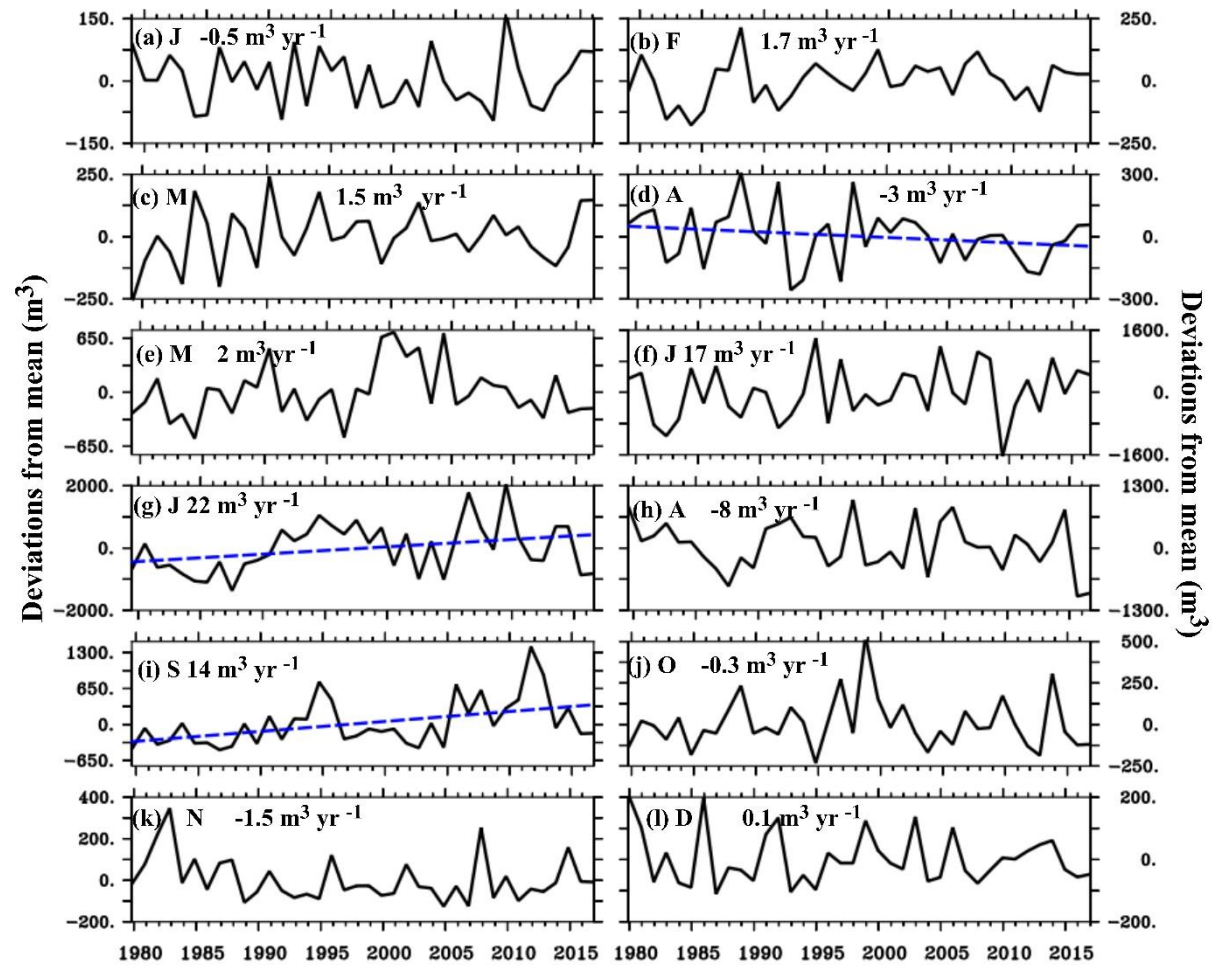


Figure 11. Monthly variations in deviations from mean of LST rates (m^3). Trend lines significant at 90% confidence interval are shown.

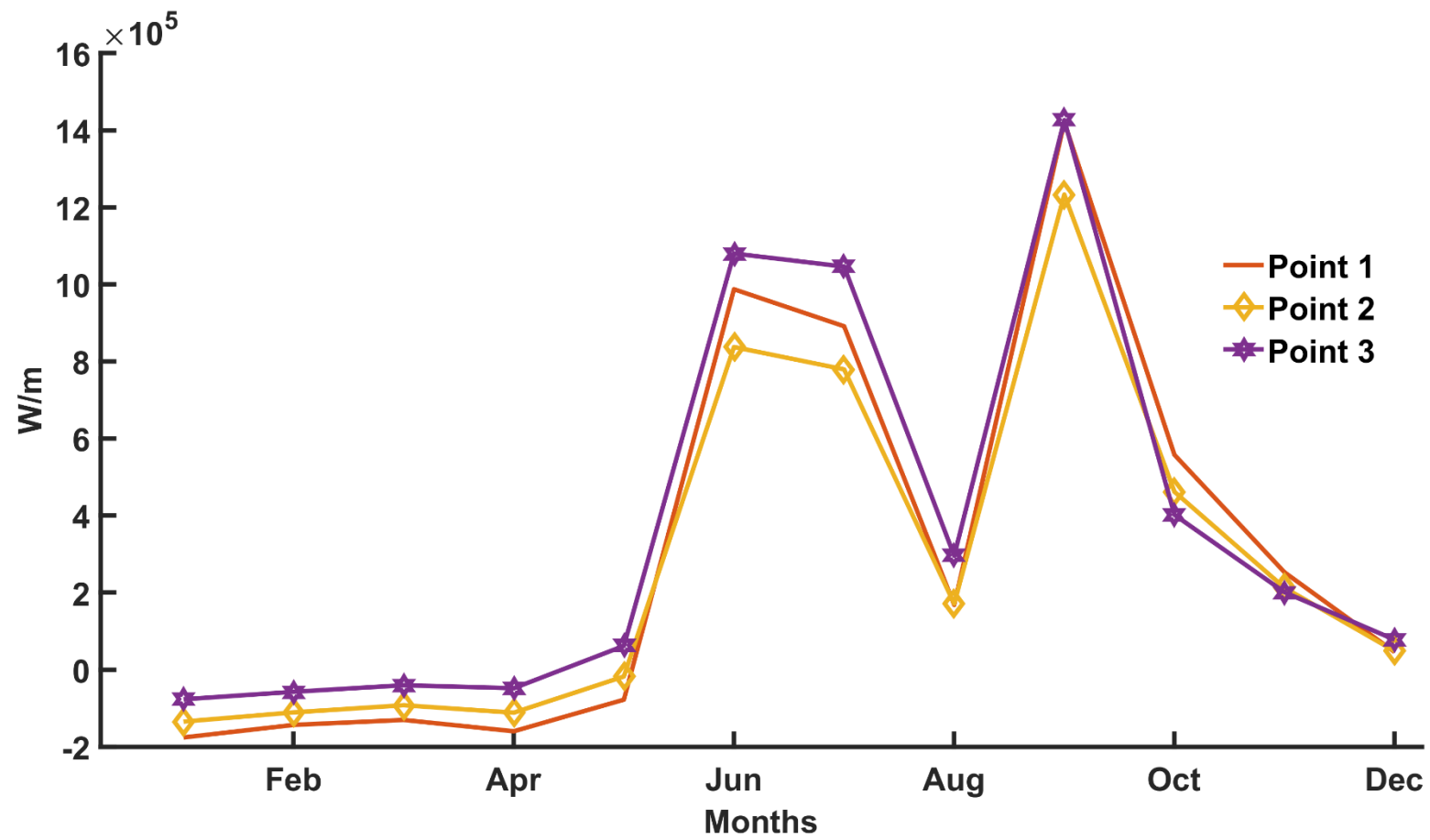


Figure 12. Monthly averaged net longshore component of wave power (W/m) along the Ganpatipule coast at 4 m water depth

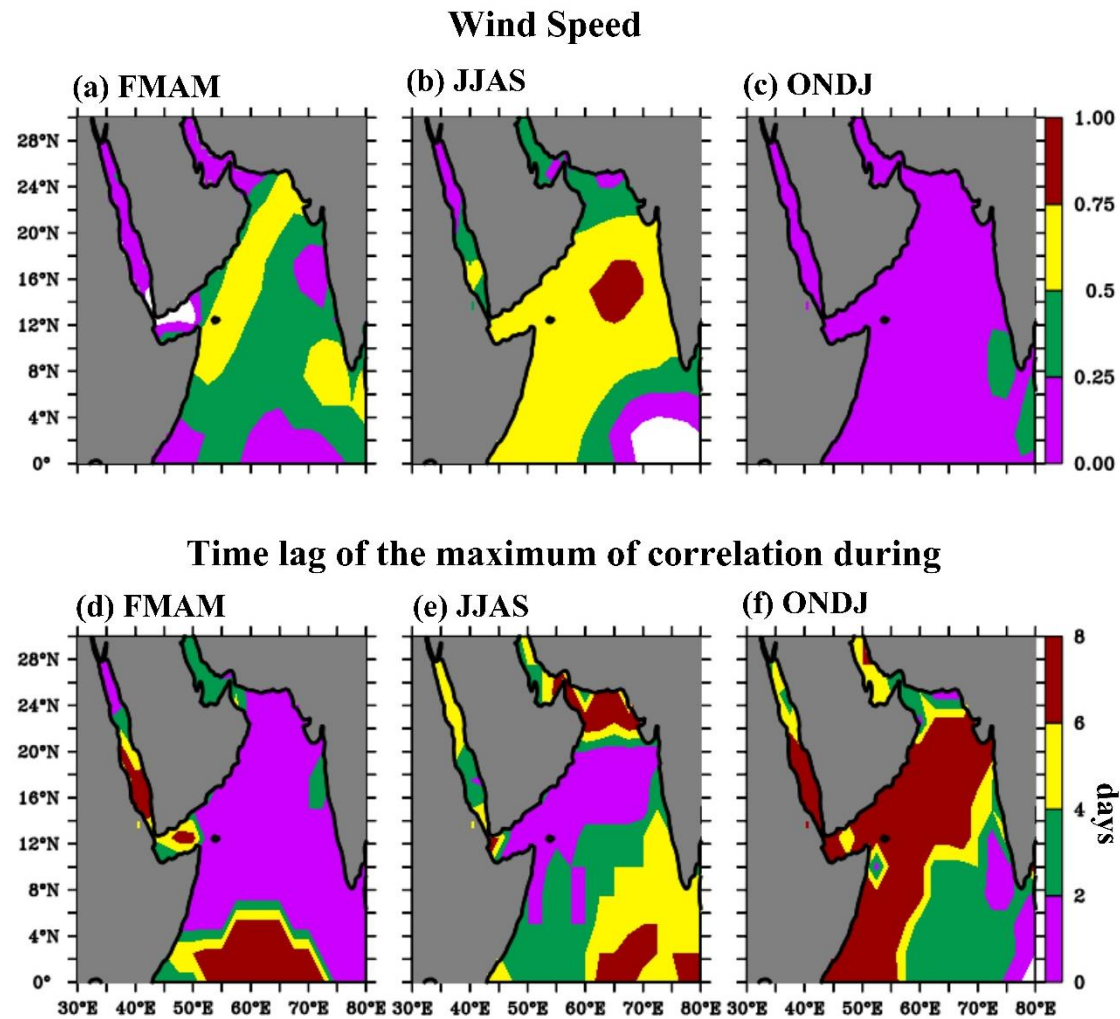


Figure 13. Maximum spatial correlation between wind speed and daily LST rates during the period 1979- 2016 of (a) FMAM, (b) JJAS, and (c) ONDJ. Time lag (d, e, f) represents the days which maximise the correlation coefficient for each grid cells

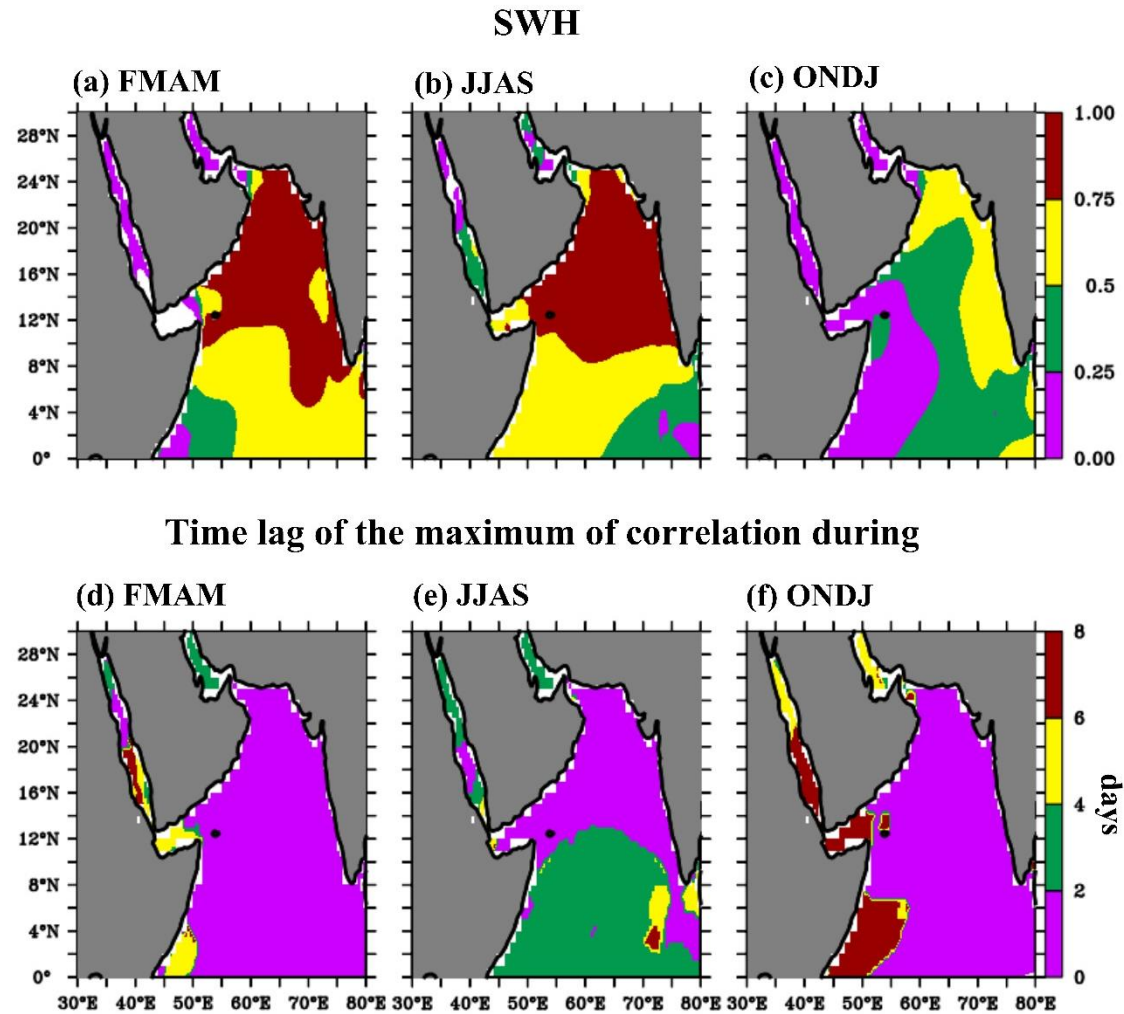


Figure 14. Maximum spatial correlation between SWH and daily LST rates during the period 1979- 2016 of (a) FMAM, (b) JJAS, and (c) ONDJ. Time lag (d, e, f) represents the days which maximise the correlation coefficient for each grid cells

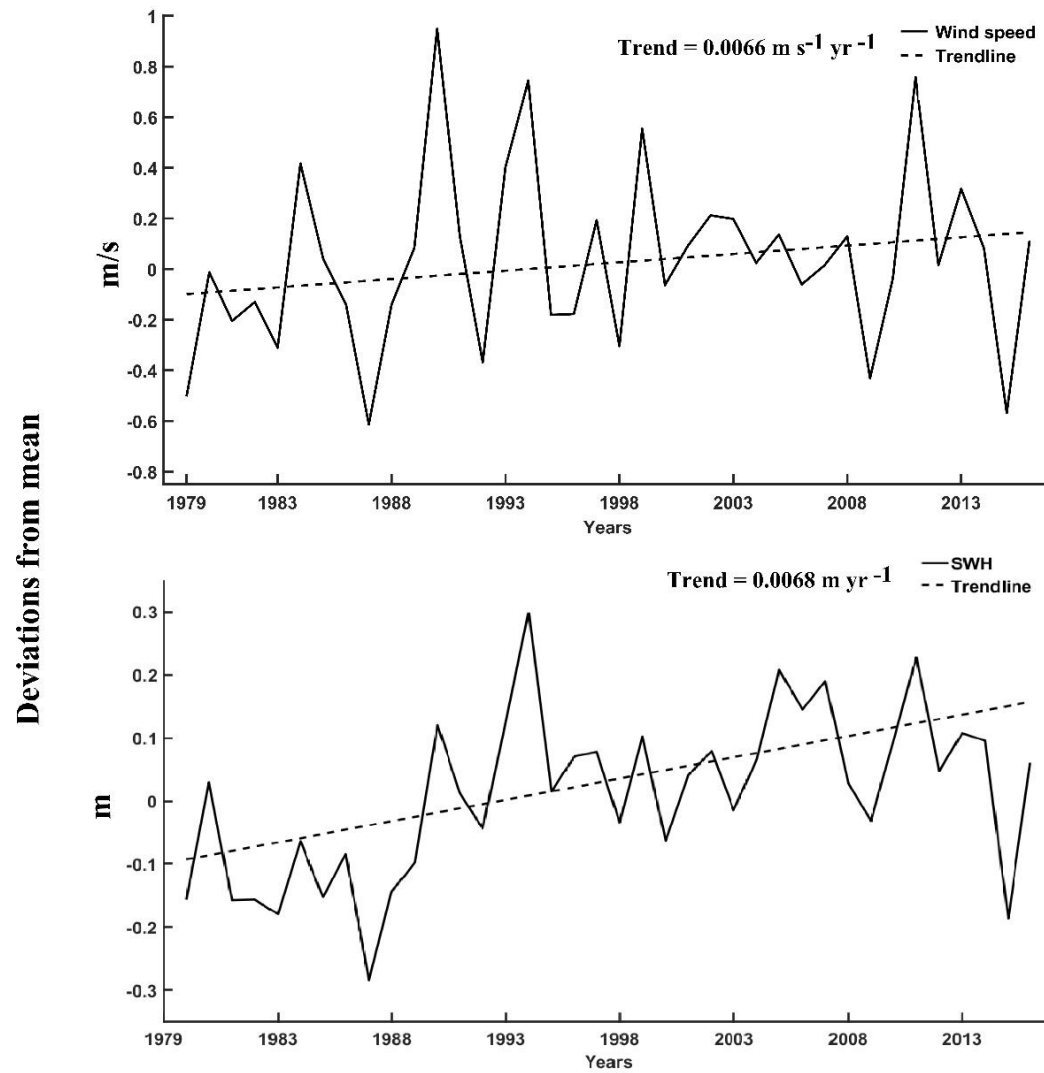


Figure 15. Deviation from mean of monsoon (JJAS) averaged wind speed and significant wave height (SWH) at the central Arabian Sea

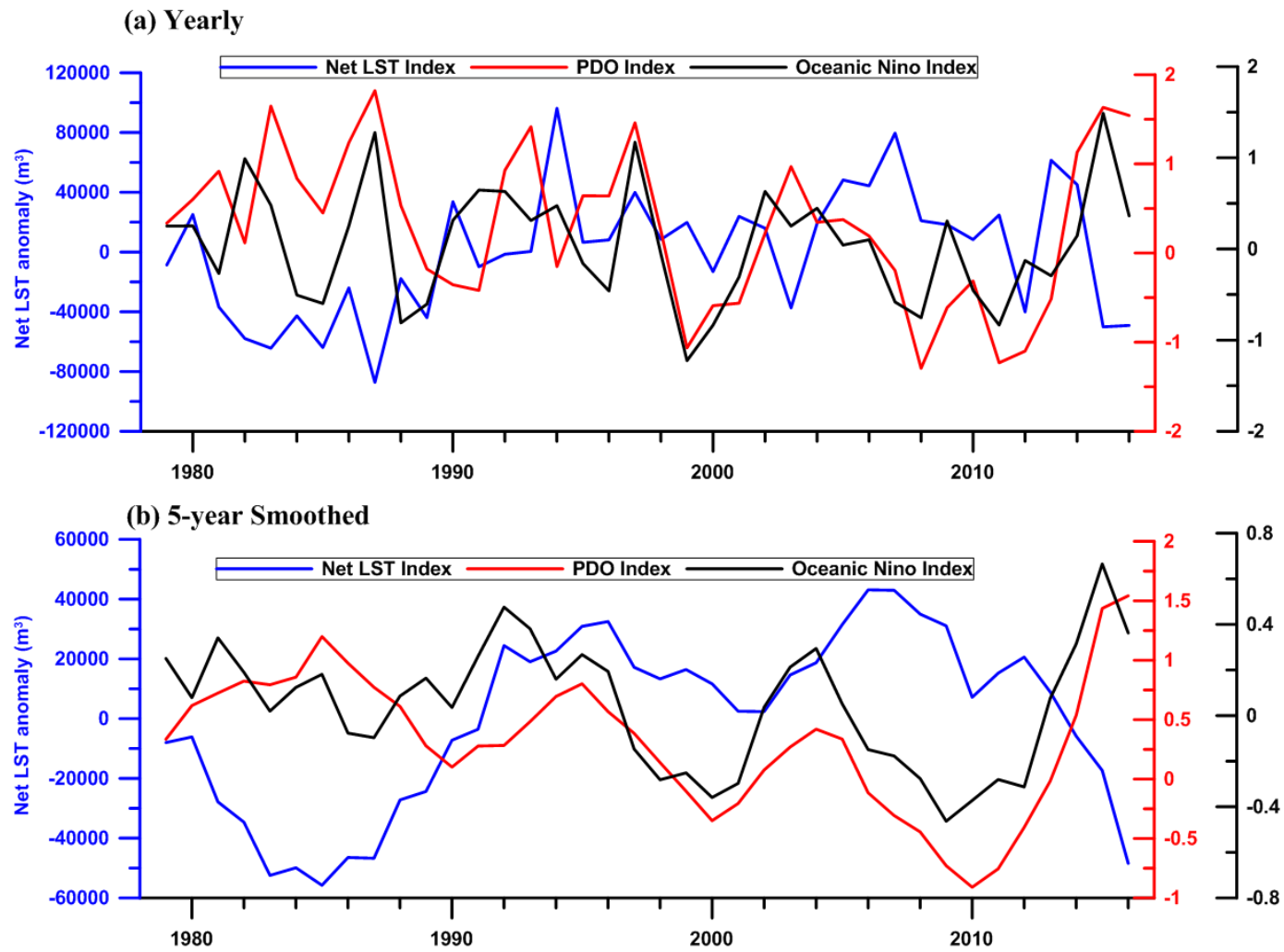


Figure 16. (a) Annual averaged and (b) 5- year smoothed indexes of PDO and ONI with net LST Index